HHS Public Access

Author manuscript

J Immunol. Author manuscript; available in PMC 2023 August 15.

Published in final edited form as:

J Immunol. 2022 August 15; 209(4): 696–709. doi:10.4049/jimmunol.2200244.

Inhibition of IL-17A Protects against Thyroid Immune-related Adverse Events while Preserving Checkpoint Inhibitor Anti-tumor Efficacy

Melissa G. Lechner[*], **Mandy I. Cheng**[†], **Anushi Y. Patel**[†], **Aline T. Hoang**[†], **Natalie Yakobian**[‡], **Michael Astourian**[†], **Marissa S. Pioso**[†], **Eduardo D. Rodriguez**[§], **Ethan C. McCarthy**[†], **Willy Hugo**[¶], **Trevor E. Angell**[‖], **Alexandra Drakaki**[#], **Antoni Ribas**[#], **Maureen A. Su**[†,**]

[*]Division of Endocrinology, Diabetes, and Metabolism, UCLA David Geffen School of Medicine, Los Angeles, CA

[†]Department of Microbiology, Immunology, and Molecular Genetics, UCLA David Geffen School of Medicine, Los Angeles, CA

[‡]Saint Louis University School of Medicine, St. Louis, MO

[§]Department of Pathology, UCLA David Geffen School of Medicine, Los Angeles, CA

[¶]Division of Dermatology, Department of Medicine, UCLA David Geffen School of Medicine, Los Angeles, CA

[‖]Division of Endocrinology and Diabetes, USC Keck School of Medicine, Los Angeles, CA

[#]Division of Hematology and Oncology, UCLA David Geffen School of Medicine, Los Angeles, CA

[**]Division of Pediatric Endocrinology, UCLA David Geffen School of Medicine, Los Angeles, CA

Abstract

Immune checkpoint inhibitor (ICI) immunotherapy leverages the body's own immune system to attack cancer cells but leads to unwanted autoimmune side effects in up to 60% of patients. Such immune related adverse events (IrAEs) may lead to treatment interruption, permanent organ dysfunction, hospitalization and premature death. Thyroiditis is one of the most common IrAEs, but the cause of thyroid IrAEs remains unknown. Here we use a new, physiologically relevant mouse model of ICI-associated autoimmunity to identify a key role for Type 3 immune cells in the

Correspondence: Dr. Melissa G. Lechner, Division of Endocrinology, Diabetes, and Metabolism, UCLA, 10833 Le Conte Ave, CHS 57-145, Los Angeles, CA, 90095. MLechner@mednet.ucla.edu; Phone: 310-794-3237.

Author contributions

M.G.L., M.I.C., T.E.A., W.H., A.D., and M.A.S. conceived the study and designed the analysis. M.G.L., M.I.C., A.Y.P., A.T.H., M.S.P., N.Y., M.A. collected the data, including mouse experiments with ICI treatment, flow cytometry, qRT-PCR, immunohistochemistry, and tumor model studies. E.C.M., W.H., A.R., A.D., and M.A.S. contributed data and analysis tools. M.G.L., M.I.C., A.Y.P., A.T.H., M.S.P., N.Y., E.C.M., W.H., and E.D.R. performed the analysis. M.G.L., M.I.C., A.Y.P., T.E.A., W.H., A.T.H., N.Y, A.D., A.R., and M.A.S. wrote or edited the paper. All authors reviewed the manuscript.

Conflict of Interest statement: A.R. has received honoraria from consulting with Amgen, Bristol-Myers Squibb, Chugai, Genentech, Merck, Novartis, Roche, Sanofi and Vedanta, is or has been a member of the scientific advisory board and holds stock in Advaxis, Appia, Apricity, Arcus, Compugen, CytomX, Highlight, ImaginAb, Isoplexis, Kalthera, Kite-Gilead, Merus, PACT Pharma, Pluto, RAPT, Rgenix, Synthekine and Tango, has received research funding from Agilent and from Bristol-Myers Squibb through Stand Up to Cancer (SU2C), and patent royalties from Arsenal Bio.

All other authors have declared that no conflict of interest exists.

development of thyroid IrAEs. Multiple lineages of IL-17A-producing T cells expand in thyroid tissue with ICI treatment. Intrathyroidal IL-17A-producing innate-like gamma delta T (γδT17) cells were increased in tumor-free mice, whereas adaptive T helper 17 (Th17) cells were also prominent in tumor-bearing mice, following ICI treatment. Furthermore, antibody-based inhibition of IL-17A, a clinically available therapy, significantly reduced thyroid IrAE development in ICI-treated mice with and without tumor challenge. Finally, combination of IL-17A neutralization with ICI treatment in multiple tumor models did not reduce ICI anti-tumor efficacy. These studies suggest that targeting Th17 and γδT17 function via the IL-17A axis may reduce IrAEs without impairing ICI anti-tumor efficacy and may be a generalizable strategy to address Type 3 immune-mediated IrAEs.

INTRODUCTION

Immune checkpoint inhibitors (ICI) against programmed death protein (PD-1) and cytotoxic T lymphocyte antigen (CTLA)-4 have revolutionized cancer therapy and hold great promise for the treatment of advanced malignancies(1). Since initial approval in 2011, eight ICI have entered clinical care, with nearly half of patients with cancer in the U.S. eligible for ICI treatment(2). ICI are used for first line therapy of metastatic renal, bladder, head and neck, liver, and certain lung, colon, and breast cancers(2). However, the benefits of ICI are limited by development of autoimmune side effects, termed immune related adverse events (IrAEs), seen in up to 60% of patients(3–5). Endocrine, gastrointestinal and liver, and dermatologic tissues are some of the most common affected by IrAEs(3, 4, 6). Pulmonary, neurologic, renal, and cardiac autoimmune side effects from ICI are less frequent but associated with grave clinical consequences, including mortality rates of 17-40%(7). IrAEs can lead to cancer therapy interruption, hospitalization, permanent organ dysfunction, and even premature death(5, 7). With the expanding use of ICIs, IrAEs represent a growing clinical problem.

Despite significant efforts to date, the mechanisms of IrAEs remain poorly understood(8). Thyroiditis is one of the most common ICI-associated IrAE, occurring in approximately 10-15% of patients treated with anti-PD1/L1 monotherapy and nearly 30% of patients treated with combination anti-PD-1/L1 and CTLA-4(6, 9, 10). As such, it may serve as a model tissue in which to study IrAE development. Like IrAEs in other organs, ICI-associated thyroiditis has both overlapping and distinct features with spontaneous thyroid autoimmunity (*i.e.* Hashimoto's thyroiditis, HT)(9–12). Similar to HT(13), a role for T cells has been shown in the pathogenesis of thyroid IrAE(14–17), including $CD4^+$ T cells and $PD1^+$ T cells. On the other hand, the pattern of ICI thyroiditis with rapid onset of gland inflammation and destruction(9, 12) is strikingly different from the smoldering autoimmunity and gradual evolution to hypothyroidism seen in HT(18).

In this study, we define immune mechanisms underlying ICI-associated thyroiditis using a new mouse model that recapitulates multiple features of IrAEs in cancer patients. Analysis of thyroid-infiltrating immune cells in ICI-treated mice revealed recruitment and activation of multiple lineages of Type 3 immune $IL\text{-}17A^+$ $ROR\gamma t^+$ T cells. Specifically, ICI treatment led to expansion of innate-like gamma delta 17 (γδT17) T cells in tumor-free mice and

adaptive $CD4^+$ helper 17 (Th17) T cells in tumor-bearing mice. Furthermore, pre-clinical studies demonstrate that IL-17A blockade effectively reduces ICI-associated thyroiditis without negatively impacting ICI-mediated anti-tumor immunity. These findings therefore point to Type 3 immune cells, previously implicated in HT(19–21) but not yet reported in thyroid IrAE, as a new target for the treatment of ICI-associated thyroid autoimmunity.

MATERIALS AND METHODS

Mice

NOD/ShiLtJ (NOD) and C57/B6 (B6) mice were obtained from the Jackson Laboratory. Male and female mice were used in equal proportions. Mice were used at 4-6-week of age unless otherwise noted. Mice were housed in a specific pathogen-free barrier facility at the University of California Los Angeles. Mice in different experimental groups were co-housed. Diabetes, determined by presence of glucose in urine (Diastix, Bayer), was assessed at least once per week and diabetic mice were treated daily with intraperitoneal insulin as described previously(22) until used in experiments or euthanized.

Cell lines

Cell lines used in these studies included MC38, a murine colon tumor model; MC38 with genetic deletion of beta 2 microglobulin (MC38.β2M$^{-/-}$); murine melanoma tumor model B16 with β2M deletion (B16.β2M$^{-/-}$)(23). Tumor cell lines were obtained from the American Type Culture Collection [(ATCC), MC38] or were gifted to Dr. Lechner and Dr. Su; (MC38.β2M$^{-/-}$ and B16.β2M$^{-/-}$ cells by Dr. Antoni Ribas). Tumor cell line authenticity was performed by surface marker analysis performed at ATCC or in our laboratory. MC38, MC38.β2M$^{-/-}$ and B16.β2M$^{-/-}$ cells were grown in complete medium [RPMI-1640 supplemented with 10% fetal bovine serum (FBS), 2mM L-glutamine, 1mM HEPES, non-essential amino acids, and antibiotics (100 U/mL Penicillin and 100 μg/mL Streptomycin)], at 37°C in humidified, 5% CO_2 incubators. Cell lines were monitored regularly for phenotype. Early passage cells were used for experiments (P1 or P2).

Reagents and media

Immune checkpoint inhibitor antibodies used were anti-mouse PD1 (clone RPM1-14), CTLA-4 (clone 9D9), and isotype controls [clone 2A3 and MPC-11, respectively] (BioXcell). For inhibitor experiments, a neutralizing antibody against mouse interleukin-17A (clone 17F3) or mouse tumor necrosis factor a (clone XT3.11), or isotype control (clone MOPC-11), were from BioXCell. Antibodies were diluted in sterile PBS for use. For *in vitro* experiments, primary immune cells were cultured in RPMI complete media [supplemented with 10% fetal bovine serum (FBS), 2mM L-glutamine, 1mM HEPES, non-essential amino acids, and antibiotics (penicillin and streptomycin)], with 50uM beta-mercaptoethanol.

Immune checkpoint inhibitor treatment of mice

Groups of 4-6 week old NOD or B6 mice were used for ICI inhibitor experiments. Mice were randomized to twice weekly treatment with anti-mouse CTLA-4 (clone 9D9), or PD-1 (RPM1-14), both anti-CTLA-4 and anti-PD-1, or an isotype control (2A3, MPC-11), at 10

mg/kg/dose intraperitoneally *(i.p.)* for four or eight weeks. During treatment mice were monitored daily for activity (including signs of neuropathy) and appearance, and twice weekly for weight and glucosuria. Mice developing glucosuria were treated with 10 units of subcutaneous NPH insulin daily. Thyroid dysfunction was assessed by measurement of free thyroxine (FT4) in sera by ELISA (LSBio). After four or eight weeks of ICI treatment (as indicated), mice were euthanized, blood collected by retro-orbital bleed, then perfused with 10mL of phosphate buffered saline (PBS). Tissues were collected for histologic analysis into neutral buffered formalin, including thyroid, lacrimal and salivary glands, lung, liver, kidney, heart, colon, eye, gonad, and pancreas. Serum was collected from blood (centrifugation 1000x*g* for 30 min). Predetermined endpoints for euthanasia before four weeks included >20% weight loss and glucosuria not resolved by insulin therapy, as per IACUC protocols.

Histology

Harvested organs were fixed in 10% buffered formalin for at least 96 hours and then stored in 70% ethanol. Organs were embedded in paraffin, sectioned (4 μm), and stained with hematoxylin and eosin (H&E) by the UCLA Translational Pathology Core Laboratory. Immune infiltration was quantified by blinded assessment of on H&E sections (5 high powered fields/section in each animal) using an adapted immune infiltrate scoring system reported previously(22). The presence of interstitial inflammation, lymphocytic aggregates, perivascular inflammation, follicular disruption, and Hurthle cell change was assessed as either present or absent on H&E tissue sections by a clinical pathologist (E.D.R.). In addition, each tissue was given an aggregate immune infiltrate score of 0 (no immune infiltrate), 1 (1-2 focal areas of immune infiltrate and/or sparse interstitial inflammation), 2 [>2 focal areas of immune infiltration, and/or presence of both focal glomerulonephritis and perivascular immune infiltration (kidney), and/or diffuse immune infiltrate affecting >25-49% of the tissue area] or 3 (diffuse immune infiltrate affecting >50% of the tissue area). For pancreas tissue, immune infiltrate score was modified as 0 for no immune infiltrate, 1 for <50% of islets affected by immune infiltration, or 2 for >50-100% of islets affected by immune infiltration. The enumeration and typing of inflammatory infiltrate were assessed through immunohistochemical stains (see below). Immune scoring was done by two blinded individuals evaluating at least 10 high powered fields per section for pancreas, lung, liver, heart, thyroid, kidney, salivary, gut (colon and stomach), and gonad tissues; for small tissues (lacrimal glands and eye) 5 high powered fields were evaluated. Images were acquired on an Olympus BX50 microscope using Olympus CellScans Standard software. Images were brightened uniformly for publication in Photoshop.

Immunohistochemistry

For immunohistochemistry (IHC), 4mm FFPE tissue sections were deparaffinized, rehydrated, and subjected to heat-induced antigen retrieval (0.01 mol/L citrate, pH 6.0) followed by treatment with 3% H_2O_2 for 10 minutes to block endogenous peroxidase activity. Sections were incubated overnight at 4°C with primary antibodies against mouse IL-17A (Abcam, ab91649, 1:50 dil), CD3 (DAKO, clone A0542, 1:100 dil), F4/80 (BioRad, clone MAC497G, 1:200 dil), B220 (BD, clone RA3-6B2, 1:50 dil). Sections were then stained with appropriate secondary antibodies and antigen detection done with 3,30-diaminobenzidine. Sections were counterstained with hematoxylin, dehydrated, and

mounted. Appropriate positive and negative controls were used for all stains. Brightness of all images was increased by 50 in Adobe Photoshop. Positively stained leukocytes for CD3, B220, F4/80, or IL-17A were counted in 10 representative high-power fields (hpf, total 400x magnification) for each tissue section. Two independent observers scored each section and the results were pooled with rare disagreements resolved by a third evaluator.

Flow Cytometry

Immediately after euthanasia and perfusion with sterile PBS, fresh tissues were dissociated for analysis of immune infiltrates by flow cytometry. Thyroid glands were dissected away from surrounding trachea and lymphoid tissue, digested in collagenase type IV (1mg/mL in 2% FBS in PBS) at 37°C for 20 minutes, then mechanically dissociated by passage through a 40um filter. Spleen cells were isolated by mechanical dissociation and passage through a 40um filter. To assess intracellular cytokines, cells were incubated in complete RPMI media with 50uM 2ME for four hours with ionomycin (1ug/mL) and PMA (50ng/mL) in the presence of Brefeldin A prior to staining. For staining, single cell suspensions were resuspended in FACS buffer (0.5mM EDTA, 2% FBS in PBS) at 10^6cells/mL and stained with fluorescence conjugated antibodies. For intracellular staining, after surface staining, cells were fixed and permeabilized using cytoplasmic fixation and permeabilization kit (BD, for cytokine IL-17A) or FoxP3 transcription factor kit (eBioscience, for RORγt), per protocol instructions, with 30 min fixation at 4°C. Viability dye DAPI was added prior to analysis where indicated. Cells were then washed twice in FACS buffer and analyzed by flow cytometry on an Attune NxT 6 cytometer (ThermoFisher). Antibodies were purchased from commercial sources Invitrogen or Biolegend (CD4, clone RM4-5; CD3, 145-2C11; CD8, 53-6.7; RORγt, AFKJS-9; IL-17A, eBio17B7; CD11c, N418; CD11b, M1/70; F4/80, BM8; B220, RA3-6B2; Nkp46, 29A1.4; TCRγδ, GL3; CD45, 30-F11). Cell counts are shown as relative frequency of live, gated single cells unless otherwise noted. For determination of infiltrating cells per thyroid lobe, absolute cell counts per thyroid lobe were determined by a calculation of cell count x fraction of thyroid analyzed to estimate a total cell count per thyroid lobe. Whole perfused thyroid specimens were dissociated to single cell suspensions and the entire specimen stained for flow cytometry and a fixed volume of the specimen was evaluated by flow cytometry to allow back calculation for estimate of absolute cell count (*e.g.* 100ul of 200ul total sample volume run yields a 2x multiplier for cell count). Typical thyroid lobe weight ranged from 0.2-0.4mg.

Immune cells were isolated from gut tissue mice to assess colitis as previously described(24). Briefly, colons were dissected from each mouse after euthanasia and perfusion as above, and cut into 1 cm pieces. Tissue pieces were first washed with 10% FBS + 2mM EDTA in PBS, underwent further mechanical dissociation with a razor blade and then digested in 1 mg/ml collagenase type IV at 37°C for 20 minutes. After digestion, cells were washed and rested in complete RPMI media to quench remaining collagenase present. Lymphocytes were isolated using Percoll gradient centrifugation. Lymphocytes were collected, washed with PBS, and used for flow cytometry analysis as above.

Neutralizing antibody studies in ICI-treated mice

Groups of 4-6 wk old NOD mice were randomized to treatment with anti-mouse PD-1 (clone RPM1-14) plus anti-mouse CTLA-4 (9D9) antibodies or isotype controls (2A3 plus MPC-11) at 10mg/kg/dose twice weekly by *i.p.* injection. Additionally, 10 days after start of ICI or isotype therapy, mice were further randomized to receive neutralizing antibody to IL-17A (clone 17F3, 0.5mg/dose) or TNFα (clone XT3.11, 0.4mg/dose), or isotype (clone MOPC-11, 0.5mg/dose), three times weekly.

Tumor model studies

Groups of 6-week old C57/B6 mice were inoculated *s.c.* with 3×10^5 MC38 tumor cells in the flank, as described previously(25). Similarly, 6-week old NOD mice were inoculated *s.c.* with 6×10^5 MC38.β2M$^{-/-}$ or B16.β2M$^{-/-}$ tumor cells in the flank. Mice were randomized into groups for treatment when tumor volumes reached 40–80mm^3. Groups of mice received anti-mouse PD-1 (clone RPM1-14), anti-mouse CTLA-4 (9D9), both, or isotype controls (2A3 plus MPC-11) at 10mg/kg/dose twice weekly, alone or in combination with a neutralizing antibody to mouse IL-17A (clone 173F, 0.5mg/dose, three times weekly) or isotype control (clone MOPC-11). Reagents were given by *i.p.* injection on the ipsilateral side to the tumor. Mouse tumor volumes were measured every 2 days by caliper and mice were sacrificed when tumor volumes exceeded 2cm in diameter or when animal morbidity mandated sacrifice under institutional vivarium protocols.

Quantitative reverse transcriptase PCR (qRT-PCR)

For RNA extraction, resected mouse thyroid lobes were snap frozen in liquid nitrogen and stored at −80°C. Multiple thyroid lobes were homogenized in RNA Lysis Buffer (Zymo Research) using the Fisherbrand 150 Handheld Homogenizer (15-340-167). RNA extractions were performed using Quick-RNA Microprep kit (Zymo Research, R1051) per manufacturer's instructions. RNA yield was quantified by nanodrop. RNA was converted into cDNA using High-Capacity cDNA Reverse Transcription Kit with RNAse Inhibitor and MultiScribe Reverse Transcriptase (Applied Biosystems, 4374966) following manufacturer's instructions. About 750 ng/uL of RNA was used for cDNA synthesis per reaction. Quantitative PCR was performed using Taqman Fast Advanced PCR Master Mix (Applied Biosystems, 4444557) and Taqman probes for genes of interest (Thermo Fisher; *Gapdh*, Mm99999915_g1; *Cd3e*, Mm00599683_m1; *Ptprc*, Mm01293577_m1; *Il17a*, Mm00439618_m1; *Il1b*, Mm00434228_m1; *Il6*, Mm00446190_m1; *Tnf*, Mm00443258_m1; *Tgfb1*, Mm01178820_m1; *Rorc*, Mm01261022_m1; *Il23r*, Mm00519943_m1), with three technical replicates per gene, per condition. PCR cycles were run using the QuantStudio 6 Pro PCR machine (Applied Biosystems) with the standard cycle parameters. Design and Analysis QuantStudio 6/7 Pro Systems Software (Thermo Fisher Scientific, Version 2.5.0) was used to identify amplification of genes and calculate fold change from Cq values. In this context, fold change was the expression ratio of the gene of interest to the housekeeping gene, GAPDH.

Single cell RNA sequencing

For mouse scRNAseq studies, $CD45^+$ infiltrating cells were isolated from fresh thyroid tissue. To reduce contamination from circulating immune cells in the blood, animals were perfused with normal saline prior to tissue collection. Thyroid tissue was enzymatically and mechanically dissociated, then single cell suspensions stained with fluorescence-conjugated antibodies to CD45, CD11b, CD3, CD4, CD8, and CD19 and viability dye DAPI. Specimens with and potential cervical thymus contamination were excluded before sequencing using a threshold of >20% double positive $CD4^+$ $CD8^+$ cells within $CD3^+$ T cells(26). Samples for each condition were then pooled to obtain sufficient cells for sequencing and analysis. Cell preparation, library preparation, and sequencing were carried out according to Chromium product-based manufacturer protocols (10X Genomics). Sequencing was carried out on a Novaseq6000 S2 2×50bp flow cell (Illumina) utilizing the Chromium single-cell 5′ gene expression library preparation (10X Genomics), per manufacturer's protocol at the UCLA Technology Center for Genomics and Bioinformatics (TCGB) Core. Data were demultiplexed and aligned with Cell Ranger version 3.0.0 or higher (10X Genomics)

Data processing of scRNA-seq libraries

After sequencing, the scRNA-seq reads were demultiplexed and aligned with Cell Ranger version 3.0.0 or higher (10X Genomics) to the mm10 (mouse) reference genome and quantified using the 10x Genomics CellRanger count software (10x Genomics). Filtered output matrices that contained only barcodes with unique molecular identifier (UMI) counts that passed the threshold for cell detection were used for downstream analysis.

Normalization, Principal Component analysis, and UMAP Clustering

Downstream analysis was done with Seurat v3 or higher(27). Only cells with a mitochondrial gene percentage less than 30% and 200 features were included in downstream analysis. Scores for S and G2/M cell cycle phases were assigned using the Seurat CellCycleScoring function following the standard Seurat pipeline(28). UMI counts were log normalized, and the top 2000 variable genes were determined using the variance-stabilizing transformation (vst) method. All genes were scaled and centered using the ScaleData function, and principal component analysis (PCA) was run for the data using the predetermined variable genes. To group cells into clusters, a K-nearest neighbors graph function (implemented in the Seurat package), followed by a modularity-optimizing function using the Louvain algorithm was used. For the cluster, 30 PC dimensions were included and the resolution parameter was set to 0.8. Cell-type clusters were visualized using uniform manifold approximation and projection (UMAP) to reduce dimensionality and allow for the cells to be visualized on a 2-D plot.

Differential Expression and Marker Gene Identification

The Seurat FindMarkers function was used to generate the top upregulated genes for each cluster using a Wilcoxon Rank Sum Test to identify differentially expressed genes across clusters. Marker genes were filtered by a minimum of detectable expression in 25% of the cells in the target group and minimum log2 fold change of 0.25. The

markers generated by these functions were compared to markers for known cell types to assign identities to the different clusters. Specifically, variably expressed gene sets for each cluster were queried in curated, publicly available databases for putative cell population identity: Enrichr(29) (https://maayanlab.cloud/Enrichr) and the Immunological Genome Project (IGP) database(30) (http://rstats.immgen.org/MyGeneSet_New/index.html). Differentially expressed genes across conditions were identified using the same function and parameters. Cells from proliferating clusters, stressed/dying clusters (expression of long non-coding RNA Malat1), thymic contamination (identity determined by Enrichr and IGP), doublets, and thyroid epithelium clusters were excluded from this analysis.

Statistics

Data were analyzed with GraphPad Prism v9. Descriptive statistics shown are mean + SEM for continuous variables. Differences in the mean frequency of immune cells or gene expression for qRT-PCR between two groups were evaluated by two-sided t test with Welch correction for potential differences in variance among groups and correction for multiple comparisons by the Holm-Sidak method. For B6 mice, differences in organ immune infiltrate score, and cell frequencies by flow cytometry were compared between groups by two-tailed, unpaired t test with Welch correction, without assumption of equal s.d. Differences in the mean frequency of immune cells, organ immune infiltrate score, cell frequencies by flow cytometry, and gene expression among groups were evaluated by Brown-Forsythe ANOVA with Welch correction for potential differences in variance among groups, followed by multiple comparisons between groups with Dunnett correction for multiple comparisons (two-tailed comparisons). Where appropriate, adjusted p values are shown. Significance was set at an alpha = 0.05. Samples sizes for each group or condition are shown.

Study approval

All experiments were conducted under UCLA IACUC-approved protocols and complied with the Animal Welfare Act and the National Institutes of Health guidelines for the ethical care and use of animals in biomedical research.

Data availability

The datasets for single cell sequencing generated and analyzed during the current study are available in the Gene Expression Omnibus (GEO) repository under accession number GSE176561 (https://www.ncbi.nlm.nih.gov/geo/).

RESULTS

The NOD background strain predisposes mice to ICI-IrAEs that mimic those seen in humans

The study of ICI-associated IrAEs has been hindered by the lack of robust preclinical models(8). While prior studies have reported autoimmunity in ICI-treated mice, these models on the C57BL/6 (B6) background developed minimal ICI-IrAEs. Augmenting these mild phenotypes required significant manipulation, such as regulatory T cell depletion(31), genetic knock-in of human checkpoint proteins(32), chemical stimulants(33)

or co-administration of complete Freund's adjuvant(34). A recent paper utilized CBA/J mice in a thyroid IrAE model, but thyroiditis induction required non-physiologic immunization with human thyroglobulin(14). We sought to develop a murine model of IrAEs that better recapitulated the development of IrAEs in patients; namely, treatment-dependent multi-system autoimmune infiltration in an immune competent host.

Patients with underlying subclinical autoimmunity or genetic predisposition have an increased risk of developing IrAEs during ICI cancer therapy(35–40). For example, patients with smoldering thyroid autoimmunity, in which thyroid peroxidase autoantibodies are present but thyroid function is still intact, were five-fold more likely to develop thyroid dysfunction during ICI therapy(11, 36, 41). Polygenetic risk scores and human leukocyte antigen variation also have been associated with increased incidence of skin, gut, and endocrine IrAEs(37–40). The NOD mouse is an autoimmune-prone strain that develops spontaneous autoimmunity in multiple tissues, including thyroiditis at low frequency (14% at 52 weeks)(42, 43). While best known for its contributions to type 1 diabetes studies, the NOD mouse has also been invaluable in understanding autoimmunity affecting other tissues(44). Given that young NOD mice, prior to the development of overt autoimmune disease, recapitulate features of patients at high risk for IrAEs, we hypothesized that NOD mice may be a robust model of ICI-associated autoimmunity. To test this, groups of four- to six-week-old NOD mice were treated twice weekly with anti-mouse CTLA-4 (clone 9D9), anti-mouse PD-1 (RPM1-14), combination (Dual ICI: anti-PD-1 plus anti-CTLA-4), or isotype control antibodies (Fig. 1a). Dual ICI-treatment was associated with an increased frequency of $CD3^+$ T cells, effector/memory ($CD44^+CD62L^-$) subsets among splenic $CD4^+$ and $CD8^+$ T cells, and regulatory T cells (Treg) compared to isotype-treated control mice (Supplemental Fig. 1a-c), consistent with prior reports(45, 46). After 4 or 8 weeks of treatment, mice were sacrificed, and salivary, lacrimal, pancreas, liver, lung, heart, colon, eye, gonad, and thyroid tissues were evaluated by histology and flow cytometry for the development of autoimmune infiltrates.

ICI-treated wild type NOD mice developed increased immune infiltrates in the thyroid gland and multiple other tissues compared to isotype-treated animals, as shown in Fig. 1b (ANOVA $p<0.0001$; p values *vs.* isotype were <0.0001 for anti-CTLA-4, anti-PD-1, and Dual ICI; $p=0.0148$ for anti-PD-1 and $p=0.0008$ for anti-CTLA-4 *vs.* Dual ICI, respectively). As in patients, autoimmunity occurred more frequently with the combination of anti-PD-1 + anti-CTLA-4 (Dual ICI) *vs.* with single agent ICI treatment (Fig. 1b). The predominant inflammation in the thyroid consisted of lymphocytic aggregates within the interstitium and occasionally perivascular aggregates (Fig. 1c). Thyroid hormone status was evaluated at 8 weeks by serum measurement of free thyroxine. A subset of dual ICI-treated mice had increased mean thyroxine serum concentrations compared to isotype controls, consistent with excess thyroid hormone release and hyperthyroxinemia during the early destructive phase of ICI-associated thyroiditis (Fig. 1d). Furthermore, some Dual ICI-treated mice notably exhibited low serum thyroxine consistent with earlier conversion to hypothyroidism over time in ICI-associated thyroiditis. Thus, this cross-sectional look at serum thyroxine levels in ICI-treated mice mirrors the dynamic transition from hyper to hypothyroidism during ICI-associated thyroiditis seen in patients (9).

Similar to ICI-treated cancer patients, thyroiditis was often seen concurrent with immune infiltrates in other tissues (*e.g.* colon, liver, lung, kidney, salivary glands), as shown in Fig. 1b and Supplemental Fig. 1d. In the liver, both focal collections of lymphocytes within liver parenchyma and peri-portal venule sites were seen. Lung tissues similarly showed aggregates of focal lymphocyte aggregation, as well as loss of alveolar air spaces. Histologic examination of the colon sections showed areas with increased immune infiltrates including basal and intraepithelial lymphocytes. The pattern of immune infiltration in the kidney was primarily glomerulonephritis with accumulation of lymphocytes and peri-vascular lymphocytic aggregates. In the pancreas, immune infiltration was centered on islet and peri-vascular areas, with lymphocytic infiltration of 25-100% of islets in most ICI-treated animals by 4 weeks. Salivary and lacrimal glands showed interstitial lymphocyte aggregates often with diffuse gland involvement. One animal developed pericardial inflammation and one had immune infiltrate in the adrenal gland. Eye, myocardial, and gonad tissues were also evaluated, and autoimmune infiltrates were not seen in any animals. As in humans(7, 47), the pattern of tissue autoimmunity showed some variation by ICI treatment (e.g. anti-PD-1, anti-CTLA-4, or combination) and may reflect differences in the inherent mechanism of tolerance in the different tissues. Notably, the rate of spontaneous autoimmunity was low in isotype-treated NOD mice, which developed only pancreatic insulitis (without diabetes) and occasional lacrimal or salivary gland focal immune infiltration at 12-15 weeks of age (Supplemental Fig. 1d), consistent with their NOD background. In summary, our mouse model recapitulates critical features of clinical ICI-associated autoimmunity seen in cancer patients, including multi-organ immune infiltration(3), and thus will facilitate studies of the mechanisms leading to IrAEs.

We also evaluated the development of autoimmune infiltrates with ICI treatment in the wild type B6 strain. As done in NOD mice, four- to six-week old B6 mice were treated twice weekly with anti-CTLA-4 and anti-PD-1 antibodies (Dual ICI) or isotype control (Supplemental Fig. 2a), and then autoimmune tissue infiltrates and thyroid autoantibodies evaluated. We chose to treat with dual ICI therapy (combination anti-CTLA-4/PD-1) since the combination has been linked with the highest rates of ICI-IrAEs(3, 4). Overall, wild type B6 mice were resistant to ICI-induced autoimmunity with immune infiltration limited on average to two organs per mouse (Supplemental Fig. 2b). Increased immune infiltrates were seen in the liver and lacrimal glands, but not in the thyroid (Supplemental Fig. 2-d). Similar results were seen in mice treated with ICI or isotype for eight weeks (data not shown). In summary, B6 mice failed to develop significant multisystem autoimmunity with combination anti-PD1 and anti-CTLA-4 immune checkpoint inhibitor (Dual ICI) therapy. These findings are in keeping with previous reports that B6 mice are resistant to spontaneous autoimmunity, perhaps due to genetic polymorphisms that alter immune responses in this inbred strain(48, 49).

T cells are the predominant cell type in thyroid immune cell infiltrate in ICI-treated mice

Thyroid IrAEs are one of the most common toxicities seen with both single agent and combination ICI(3, 6). Furthermore, ICI-associated thyroiditis frequently leads to permanent thyroid gland destruction requiring lifelong hormone replacement even after discontinuation of immunotherapy(12). Thus, we selected the thyroid as a model tissue to understand

mechanisms of ICI-associated autoimmunity. We found evidence of thyroiditis in 7/10 NOD mice treated with Dual ICI (Fig. 1b), suggesting that NOD mice are a robust model for understanding the mechanism(s) underlying thyroid-IrAEs. Therefore, we focused next on defining immune changes occurring with ICI-associated thyroid autoimmunity in our model. We measured the frequency of different immune populations in thyroid specimens from ICI- *vs.* isotype-treated mice (Fig. 2a). Expression of *Ptprc,* a marker of hematopoetically derived cells, and *Cd3e,* a T cell lineage marker, assessed by quantitative reverse transcriptase polymerase chain reaction (qRT-PRC) were significantly increased, consistent with increased thyroid immune cell infiltration, notably T cells, with ICI treatment (Fig. 2b). Immunohistochemistry (IHC) staining for canonical immune markers on FFPE thyroid sections showed the presence of T cells (CD3), macrophages (F4/80), and B cells (B220) in immune aggregates in ICI-treated mice, with rare immune cells in the thyroid parenchyma of isotype controls (Fig. 2c). To quantify the types of immune cells in thyroid tissue of ICI- vs. isotype treated NOD mice, we used flow cytometry, as shown in Fig. 2d and 2e (gating strategy in Supplemental Fig. 1e). Fresh thyroid tissues from ICI or isotype-treated mice were perfused with saline to remove circulating peripheral immune cells and dissociated into single cell suspensions then stained for immune markers and analyzed for $CD45^+$-gated immune cells. T cells ($CD3^+$) constituted the major group of the infiltrating immune cells ($CD45^+$) in thyroid tissue and were significantly increased in ICI-treated mice (mean 3,332±1,220 cells/thyroid lobe *vs.* 420±176, p=0.027) (Fig. 2e). Other populations seen in thyroid immune infiltrates were also more numerous in ICI-treated mice, including dendritic cells (DC; $CD11c^+$ $CD3^-$ $F4/80^-$ $B220^-$ $CD11b^{low}$, mean 46±9 *vs.* 16±5, p=0.008; $CD11c^+$ $CD3^-$ $F4/80^-$ $B220^-$ $CD11b^+$ mean 214±37 *vs.* 73±13, p=0.001), B cells ($B220^+$ $CD3^-$ $CD11b^-$, mean 212±77 *vs.* 32±13, p=0.03), and natural killer (NK) cells ($NKp46^+CD3^-$, mean 221±74 *vs.* 46±16, p=0.03) (Fig. 2e). While macrophages were present in thyroid immune infiltrates, we did not find a significant difference in mean intrathyroidal macrophage number between ICI- and isotype-treated mice ($F4/80^+$, mean 182±33 *vs.* 130±21, p=0.21) (Fig. 2e). In summary, these data show a T cell predominant, but diverse, thyroid immune cell infiltrate associated with ICI-treatment in our mouse model.

Evidence for a role for Type 3 immunity in ICI-mediated thyroiditis

T cells have been clearly implicated in thyroid IrAEs(14–16), but are also the primary target and effector population for anti-cancer effects of ICI(1). Therein arises the challenge in preventing IrAEs in cancer patients on ICI therapy. However, recent data in gut ICI-induced IrAEs suggested that immune adverse events may be uncoupled from anti-cancer efficacy using anti-inflammatory treatments(50). Therefore, we sought to identify T cell subsets that may play a key role in thyroid autoimmunity but may not be necessary for anti-tumor efficacy. Prior studies have shown that Type 3 immune responses, namely interleukin-17 producing T cells, are critical in the pathogenesis of spontaneous thyroid autoimmunity (*e.g.* HT)(19–21, 51). However, the role of Type 3 immunity has not yet been described in ICI-associated thyroiditis. Central to Type 3 immune responses is *Rorc,* which encodes RORγt, a master transcriptional regulator that drives expression of IL-17 cytokines in multiple cell types(52, 53). *Il23r* encodes the receptor for IL-23, a cytokine that stimulates T cell IL-17 production and has been linked with multiple autoimmune diseases, including colitis, psoriasis, and inflammatory arthritis(54). Based upon its association with HT, we

reasoned that Type 3 immune responses might also underlie autoimmune pathogenesis in ICI-associated thyroiditis.

We used qRT-PCR to compare the relative intrathyroidal gene expression of Type 3 immune response-associated genes in whole, saline-perfused thyroid tissue from ICI- *vs.* isotype treated NOD mice. As shown in Fig. 3a, expression was significantly increased in Dual ICI treated mice for *Rorc* [mean fold change (FC) 2.4±0.1, p<0.001], *Il23r* (FC 1.28±0.09, p<0.001), and *Il17a* (FC 1.45±0.07, p<0.001)]. Cytokines previously shown to promote IL-17-producing $CD4^+$ T helper (Th17)(51) differentiation (TGFβ and IL-6) and γδT17 activation (TNFα)(55) were also increased in thyroids of ICI-treated mice compared to isotype-treated animals (Fig. 3a). In addition, flow cytometry analysis of thyroid immune infiltrates showed increased intrathyroidal $ROR\gamma t^+$ $CD3^+$ T cells [inclusive of $CD4^+$ Th17(51), $CD8^+$ T effector (Tc17)(56), and γδT17(55) subsets], in Dual ICI-treated mice compared to isotype controls (mean 936±267 *vs.* 183±43 cells per thyroid lobe, p=0.010, Fig. 3b). To better characterize $ROR\gamma t^+$ and IL-17A-producing populations in thyroid immune infiltrates of ICI-treated mice, we quantified different $IL\text{-}17A^+$ cell subsets: $CD4^+$ Th17, $CD8^+$ Tc17(56), and γδT17 cells (Fig. 3c, with additional gating strategy shown in Supplemental Fig. 1e). Pan-$CD3^+$ $IL\text{-}17A^+$ cells (including αβTCR $CD4^+$ and $CD8^+$ and γδTCR subsets) were increased in the thyroids of mice ICI-treated mice (Fig. 3d, mean 13± SEM 8 cells per thyroid lobe in isotype-treated *vs.* 79±12 in anti-CTLA-4 *vs.* 45±10 in anti-PD-1, 79±15 in Dual ICI; ANOVA p<0.001; p values for comparison to isotype were anti-CTLA-4 0.002, anti-PD-1 0.07, Dual ICI 0.01). Among $IL\text{-}17A^+$ T cell subsets (Fig. 3e), γδT17 cells were significantly increased in thyroid immune infiltrates following ICI treatment (8±5 cells per thyroid lobe in isotype-treated *vs.* 50±5 in anti-CTLA-4 *vs.* 34±4 in anti-PD-1, 41±8 in Dual ICI; ANOVA p<0.0001; p values for comparison to isotype were anti-CTLA-4 <0.001, anti-PD-1 0.003, Dual ICI 0.02). Th17 and Tc17 cells were not significantly different in ICI-treated groups compared to isotype controls (Fig. 3e). Rare $CD3^-$ $IL\text{-}17A^+$ cells were seen in intrathyroidal immune infiltrates by flow cytometry, which may represent macrophages or innate lymphoid cells type 3 (ILC3)(57). In summary, these data suggest a potential role for $ROR\gamma t^+$ IL-17A-producing T cells in not only spontaneous thyroiditis, as has been previously reported(19, 21), but also ICI-associated thyroiditis.

scRNAseq demonstrates a prominent γδ17 population among diverse immune cell types in thyroid infiltrate

A major challenge with studying thyroiditis in mouse models is the diminutive size (average volume= 4.92 μL(58)) of the thyroid organ. To delineate immune cell types at single cell resolution in thyroid autoimmune infiltrates in our mouse model, we turned to single cell RNA sequencing (scRNAseq; Fig. 3f). Sorted, live $CD45^+$ cells from thyroid specimens of NOD mice treated with combination anti-PD-1 and anti-CTLA-4 (Dual ICI, n=16 mice) or isotype control (n=10 mice), were used to construct Chromium™ 10x single cell 5' gene expression libraries for single cell sequencing. Immune cell populations were identified and visualized by UMAP (Fig. 3g total n=8,596 cells, with 7,700 cells from Dual ICI and 896 cells from isotype). Putative cell cluster identities in Fig. 3g were assigned using publicly available curated databases (Enrichr(29) and the Immunological Genome Project database(30); full gene lists provided in **Dataset I**). Specifically, lymphoid cell clusters

consisted of CD4$^+$ T cells (Cd4: *Cd3e, Cd4*), CD8$^+$ T cells (Cd8: *Cd3*, *Cd8a*), and gamma delta (γδ) T cells (*Cd3e, Trdc, Trg-V6/V4/V1*). CD4 T cell clusters were further defined as Treg *(Cd3e, Cd4, Foxp3, Ctla4, Ikzf2),* two putative Th1 populations (*Tbx21, Ifng*) expressing effector (*Icos, Gzmk*) or exhaustion markers (Cluster 16: *Pdcd1, Ctla4*), CD40L$^+$ CD4 (*CD4, Cd40lg*), two memory populations (Cluster 8: T effector memory, TEM; Cluster 15: T central memory, TCM), and naïve CD4 T cells (Cluster 0: *Ccr7, Sell, Lef1*). CD8 T cell populations included a population defined by IFNγ$^+$ CXCR6$^+$ and cytotoxicity (Cluster 10: *Prf1, Gzmk, Fasl, Ifng*, *Cxcr6*) and a cluster containing naïve and memory CD8 T cells (Cluster 3: *Ccr7, Sell, Il7r, Lef1*). γδT cells were found in two clusters, with a γδT17 subset (Cluster 5: *Rorc*$^+$ *Tcrg-V6*$^+$ and *Trcg-V4*$^+$ γδT) and a cytotoxic IFNγ$^+$ γδT subset (Cluster 7: *Tbx21*$^+$ *Ifng*$^+$ *Gzmb*$^+$ *Tcrg-V1*$^+$ and *Trcg-V4*$^+$ γδT). Cluster 7 also included NK and NKT cells (*Ncr1, Cd7, Nkg7, Klrd1, Tbx21*). Type 1 immune responses (*i.e. Ifng, Tbx21*) and cytotoxic T cells have previously been reported in ICI treatment and are thought to be important for anti-tumor effects(59, 60). Other immune cell clusters included macrophages and monocytes (Clusters 9 and 14, respectively: *Cd68, Cd14, Fcgr1, Adgre1, C1qa/b/c, Csfr1, Cd74*), conventional DC (Cluster 17, cDC: *Cd14, Itgax, H2-Aa*), ILC type 2 (Cluster 11, ILC2: *Il7r, Il1rb, Il13, Il5, Fosb*), B cells (Cluster 13, *CD19*, *Bank1*, *Msa41*, *Cd79a, Cd19, Cd74, Igkc*), and two comprised of mixed immune cell types segregated primarily by *Mik67* and *Ccna2*, consistent with proliferating cell populations (4 and 12). Expression of key immune cell genes for each cluster is shown in Supplemental Fig. 3a. UMAP projections split by condition demonstrated that cells originating from either isotype-treated or dual ICI-treated thyroids were present in each cluster (Fig. 3h). Notably, mean numbers of immune cells per thyroid were higher in ICI-treated mice compared to isotype-treated (Supplemental Fig. 3b). Thus, while the composition of immune cells in ICI- and isotype-treated thyroids were similar, these findings suggest that immune cell populations are highly expanded with ICI treatment.

Type 3 immunity genes, including *Rorc* and *Il23r*, were also seen in scRNAseq of intrathyroidal immune cells from ICI and isotype-treated NOD mice (Fig. 3i), with highest expression in Cluster 5 comprised of γδT cells (Supplemental Fig. 3c). Cells in this *Rorc*$^+$ *Il23r*$^+$ cluster also expressed *Cd3e, Il17a*, *Trdc, Tcrg-V6, Serpinb1a, Tmem176a, and Tmem176b,* supporting their inclusion of IL-17-producing gamma delta T cells (γδT17) (Supplemental Fig. 3c)(55, 61). The presence of *Rorc*$^+$ *Il23r*$^+$ T cells in isotype treated mice (Fig. 3i) may reflect low levels of spontaneous thyroid autoimmunity previously described in NOD mice(42, 44). Thus, our scRNAseq data corroborate flow cytometry data (Fig. 3e) which also demonstrate a prominent γδT17 population in ICI-associated thyroiditis infiltrates. Finally, scRNAseq data showed expression of myeloid cell attracting IL-17A driven chemokines, including CXCL1, CXCL2, and CCL2 (Supplemental Fig. 3d), highlighting a potential pathway by which T cell-derived IL-17A may contribute to the diverse immune cell infiltrate seen in thyroiditis.

IL-17A neutralizing antibody reduces autoimmune infiltrates in ICI-treated mice

Based on these data, we predicted that blocking IL-17A could reduce thyroid autoimmunity in ICI-treated mice. Strategies for blocking IL-17A have been developed for multiple autoimmune indications(62) and could be readily applied to reduce ICI-associated IrAEs

in patients with cancer. We therefore tested the effects of an IL-17A neutralizing antibody (clone 17F3, 0.5mg/dose 3x/week *i.p.*) begun 10 days after Dual ICI therapy in NOD mice (Fig. 4a). Indeed, this IL-17A neutralizing antibody reduced the frequency and severity of autoimmune infiltrates, including thyroiditis, in ICI-treated mice at 4 weeks (Fig. 4b; ANOVA $p<0.0001$ for immune infiltrate; p values *vs.* isotype were Dual ICI <0.0001 and Dual + αIL-17A 0.005; p value Dual ICI vs Dual + αIL-17A 0.003). The incidence of autoimmune infiltrates across tissues with Dual ICI vs Dual + αIL-17A for individual mice is shown in Fig. 4b (data from two representative experiments), including thyroid (14/14 vs 2/9 mice with immune infiltrate), colon (13/16 vs 7/10), lung (15/16 vs 4/10), and liver (10/16 vs 1/16). By histological examination, ICI-associated thyroid immune infiltrates were reduced with the addition of anti-IL-17A antibody (Fig. 4c). By flow cytometry analysis (Fig. 4d, gating strategy shown in Supplemental Fig. 1e), thyroid infiltrating $CD45^+$ immune cells were reduced from mean 16,251± SEM 6,068 cells/lobe in Dual ICI-treated mice, to 339±133 in Dual ICI with anti-IL-17A, and compared to 3,389±2,273 in isotype-treated mice (ANOVA $p<0.03$; p values *vs.* isotype were Dual ICI 0.18 and Dual + αIL-17A 0.35; p value Dual ICI vs Dual + αIL-17A 0.045). Thyroid-infiltrating $CD3^+$ T cells were reduced as well, mean 4,031±1,167 cells/thyroid lobe in Dual ICI *vs.* 164±59 with Dual ICI + αIL-17A *vs.* 651±229 with isotype (ANOVA $p=0.001$; p values *vs.* isotype were Dual ICI 0.02 and Dual + αIL-17A 0.0.14; p value Dual ICI vs Dual + αIL-17A 0.008). Other thyroid-infiltrating immune cell populations evaluated were also decreased, including B cells (mean 212±77 cells/thyroid lobe in Dual ICI *vs.* 20±10 in Dual ICI + αIL-17A *vs.* 32±13 in isotype, ANOVA $p=0.01$; p values *vs.* isotype were Dual ICI 0.09 and Dual + αIL-17A 0.86; p value Dual ICI vs Dual + αIL-17A 0.06), NK cells (mean 222±75 cells/thyroid lobe in Dual ICI *vs.* 16±4 in Dual ICI + αIL-17A *vs.* 46±16 in isotype, ANOVA $p=0.009$; p values *vs.* isotype were Dual ICI 0.09 and Dual + αIL-17A 0.27; p value Dual ICI vs Dual + αIL-17A 0.04), $CD11c^+CD11b^{low}$ DC (mean 42±9 cells/thyroid lobe in Dual ICI *vs.* 8±2 in Dual ICI + αIL-17A *vs.* 11±3 in isotype, ANOVA $p<0.001$; p values *vs.* isotype were Dual ICI 0.008 and Dual + αIL-17A 0.92; p value Dual ICI vs Dual + αIL-17A 0.005), and $CD11c^+CD11b^+$ DC (mean 214±39 cells/thyroid lobe in Dual ICI *vs.* 46±10 in Dual ICI + αIL-17A *vs.* 67±13 in isotype, ANOVA $p<0.001$; p values *vs.* isotype were Dual ICI 0.006 and Dual + αIL-17A 0.50; p value Dual ICI vs Dual + αIL-17A 0.002). Controls treated with isotype + αIL-17A showed infiltrates comparable to isotype-only controls (data not shown). In summary, inhibition of IL-17A effectively decreases autoimmune thyroid infiltration during ICI treatment.

Our transcriptional data also showed intrathyroidal accumulation of immune cells expressing *Tnf*, a pro-inflammatory cytokine important in the differentiation of γδT17 and Th17 cells(55, 63) (Fig. 3a and Supplemental Fig. 4a). *Tnf* expression was seen by monocytes and macrophages (Clusters 9 and 14) and intrathyroidal T cells (including γδT17, $CD4^+$ and $CD8^+$ subsets) (Supplemental Fig. 4a). Interestingly TNFα has previously been implicated in patients with ICI-associated colitis(64) and Perez-Ruiz *et al.*(50) showed that prophylactic TNFα blockade reduced the incidence of colitis during ICI therapy in a mouse model. Given its role in the IL-17A axis and efficacy in preventing ICI-associated colitis, we also evaluated the effects of a TNFα neutralizing antibody (clone XT3.11, 0.4mg/dose 3x/week *i.p.*) begun 10 days after anti-PD-1 + anti-CTLA-4 ICI therapy (Supplemental Fig. 4b). A

TNFα neutralizing antibody significantly reduced immune infiltrates across multiple tissues in our mouse model of ICI-associated autoimmunity (Supplemental Fig. 4c) and reduced thyroid autoimmune cell infiltrates (Supplemental Fig. 4d). These data are consistent with previously published findings(50, 64) and provide further validation of this model as a tool to identify strategies to reduce IrAEs. In summary, inhibition of the IL-17A axis (via IL-17A or TNFα blockade) effectively reduces thyroid autoimmune infiltrates with ICI treatment.

Evaluation of ICI-associated thyroid autoimmunity in tumor-bearing NOD mice

We next evaluated thyroid autoimmunity in tumor-bearing NOD mice to test whether the observed increase in IL-17A$^+$ T cells with ICI treatment were also seen in the context of a cancer. Few syngeneic tumor models have been developed on the NOD background(65), though several are actively in development by us and others(66). Therefore, we utilized two B6 tumor models with beta-2 microglobulin (β2M) deletion(23). Rejection of allogeneic tumor models is due largely to expression of non-syngeneic major histocompatibility receptors (MHC) and we hypothesized that tumor models with a deficit of MHC class I expression would grow in immune competent NOD mice. In addition, MHC class I deficient tumors are commonly seen in patients since loss of MHC class I expression is a frequent mechanism of immune escape(23, 67, 68). Both tumor models successfully grafted to palpable tumors in NOD mice (Fig. 5), thus providing two cancer cell lines for testing ICI effects in NOD mice.

Groups of NOD mice were inoculated with B16.β2M$^{-/-}$ melanoma or MC38.β2M$^{-/-}$ colon carcinoma tumor cells. Once tumors reached a threshold size, mice were treated with Dual ICI or isotype control antibodies for 4 weeks (Fig. 5a). Thyroids from Dual ICI-treated vs. isotype-treated tumor-bearing mice were examined for immune infiltrate by flow cytometry. Intrathyroidal pan-CD3$^+$ IL-17A$^+$, and Th17, Tc17, and γδT17 subsets (Fig. 5b) were quantified using flow cytometry. In mice with B16.β2M$^{-/-}$ or MC38.β2M$^{-/-}$ tumors, intrathyroidal CD3$^+$ IL-17A$^+$ cells were increased with Dual ICI-treatment compared to isotype control ($p<0.05$ and $p<0.005$, respectively, Fig. 5b). Interestingly, in mice with B16.β2M$^{-/-}$ tumors, Th17 and Tc17 cells were increased ($p<0.05$ for both); γδT17 cells showed a trend for increase that was not significant ($p=0.0519$). Similarly, in Dual ICI-treated mice bearing MC38.β2M$^{-/-}$ tumors, there was a significant increase in intrathyroidal Th17 cells ($p<0.05$). In summary, while innate-like γδT17 cells are the primary IL-17A$^+$ subset in thyroid infiltrates with ICI treatment in tumor-free mice, ICI-induced thyroid immune infiltrates in tumor-bearing mice are dominated by increased adaptive Type 3 immune responses (*i.e.* Th17 and Tc17 cells).

One advantage to targeting IL-17A for the prevention of thyroid IrAEs, is that it may inhibit the actions of both adaptive (Th17, Tc17) and innate (*e.g.* γδT17) Type 3 immune cells. We tested whether IL-17A neutralizing antibody therapy could also reduce thyroid autoimmune infiltrates during Dual ICI treatment in tumor-bearing mice (Fig. 5c). Groups of NOD mice bearing B16.β2M$^{-/-}$ melanoma or MC38.β2M$^{-/-}$ colon tumors were treated with Dual ICI or isotype, and αIL-17A or isotype (mock), and then thyroid infiltrating immune cells were assessed by flow cytometry after 4 weeks. αIL-17A reduced the frequency and severity of thyroid T cell autoimmune infiltration in ICI-treated mice (Fig. 5d). Thyroid infiltrating

$CD3^+$ T cells in ICI-treated mice with B16.$\beta 2M^{-/-}$ melanoma were reduced from mean 2,089± SEM 542 cells/lobe in Dual ICI-treated mice, to 568±241 in Dual ICI with αIL-17A, compared to 163±47 in isotype control (ANOVA p=0.0008; p values *vs.* isotype were Dual ICI 0.0058 and Dual + αIL-17A 0.3349; p value Dual ICI vs Dual + αIL-17A 0.0472). In ICI-treated mice with MC38.$B2M^{-/-}$ colon tumors, thyroid infiltrating $CD3^+$ T cells were reduced from mean 4,274± SEM 1,237 cells/lobe in Dual ICI-treated mice, to 403±169 in Dual ICI with αIL-17A, and compared to 442±223 in isotype control (ANOVA p=0.0009; p values *vs.* isotype were Dual ICI 0.0155 and Dual + αIL-17A 0.9986; p value Dual ICI vs Dual + αIL-17A 0.0140). These data support a pathogenic role for IL-$17A^+$ T cells in the development of Dual ICI-associated thyroid autoimmune infiltrates and further demonstrate the potential benefit for IL-17A blocking therapy in reducing ICI-associated thyroid immune infiltrates.

Role of IL-$17A^+$ T cells in ICI-associated autoimmune infiltrates in other tissues

Similar to cancer patients who often develop IrAEs across multiple tissues(5), ICI-treated NOD mice develop autoimmune infiltrates in multiple organs (Fig. 1). However, different tissues may have distinct inherent mechanisms of immune tolerance. Given the role of IL-17A in ICI-thyroiditis and multiple spontaneous autoimmune diseases, we hypothesized that IL-17A may contribute to the development of ICI-associated immune infiltrates in other tissues. IL-17A has previously been implicated in the development of inflammatory bowel disease, a spontaneous autoimmune disease affecting the gastrointestinal system(51). Importantly, colitis is the second most common IrAE seen in patients, manifesting with diarrhea, weight loss, bloody stool, and even gut perforation(3, 7, 69). As such, it represents a major clinical challenge to ICI use. In our ICI-treated mice, gut autoimmunity may manifest as weight loss, bloody stools, and gut immune cell infiltration. We assessed the presence of IL-$17A^+$ T cells in the gut of ICI-treated NOD mice using flow cytometry (Supplemental Fig. 4e, gating strategy same as for thyroid specimens). IL-$17A^+$ $CD3^+$ T cells were present in the gut of isotype and Dual ICI-treated mice in tumor bearing mice, comprising approximately 15-20% of colon $CD45^+$ cells (Supplemental Fig. 4e). IL-$17A^+$ T cells were comprised primarily of $CD4^+$ Th17 cells, with rarer Tc17 and γδT17 cells. Interestingly, while there was not a significant difference in the frequency of IL-$17A^+$ T cells in the colon between Dual ICI and isotype treated, treatment with an IL-17A neutralizing antibody significantly reduced the frequency and extent of colon autoimmune infiltrates (Supplemental Fig. 4f). This may reflect changes in activation, rather than accumulation or proliferation, of IL-$17A^+$ T cells in the colon with ICI treatment.

The NOD mouse develops spontaneous autoimmune diabetes mellitus, and ICI treatment accelerated insulitis and the onset of diabetes. Rare IL-$17A^+$ $CD3^+$ cells were found in the pancreas of both isotype and ICI-treated mice with no significant difference seen between conditions (Supplemental Fig. 4g). Neutralizing IL-17A therapy did not delay the onset of autoimmune diabetes (Supplemental Fig. 4h) in ICI-treated mice. In summary, these data suggest that IL-17A contributes to the development of ICI-associated autoimmunity in a tissue-specific manner.

IL-17A neutralizing antibody during ICI treatment does not reduce anti-tumor effects

Our data suggested that a neutralizing IL-17A antibody may reduce ICI-associated thyroid autoimmune infiltration in both tumor-free and tumor-bearing mice. In developing therapies to prevent or reduce IrAEs in patients, it will be critical that any approach preserve the anti-tumor immune effects of ICI. Recent reports have shown a correlation between the development of thyroid IrAEs and improved tumor response to ICI therapy(70–72). Thus, it is possible that some components of the immune response contributing to ICI-autoimmunity may overlap with those required for effective anti-tumor immunity. Whether IL-17A inhibition may have deleterious effects on the efficacy of ICI treatment in anti-tumor immunity is unclear, since IL-17A has been associated with pro-tumorigenic effects in some cancers(57, 73–75) and anti-tumorigenic effects in others(57, 73, 74). To test this, we determined the effect of IL-17A blockade during ICI treatment on the growth of tumors in NOD mice. Dual ICI treatment of B16.β2M$^{-/-}$ melanoma and MC38.β2M$^{-/-}$ colon tumors in NOD mice significantly reduced tumor growth (Fig. 5e). Importantly, the addition of αIL-17A did not reduce the anti-tumor effect of ICI treatment (Fig. 5e; ANOVA for day 25 tumor volume in B16.β2M$^{-/-}$ p=0.0029; p values for comparison to isotype were Dual ICI 0.0226, Dual ICI + αIL-17A 0.0286. No significant difference between Dual ICI *vs.* Dual ICI + αIL-17A, p=0.9403; ANOVA comparing day 25 tumor volume in MC38.β2M$^{-/-}$ p=0.0004; p values for comparison to isotype were Dual ICI 0.0043, Dual ICI + αIL-17A 0.0042. No significant difference between Dual ICI *vs.* Dual ICI + αIL-17A, p=0.94). Neutralizing IL-17A antibody therapy combined with Dual ICI treatment of syngeneic MC38 colon tumors in B6 mice also showed no loss of anti-tumor efficacy compared to Dual ICI with a mock isotype control (Fig. 5f). In summary, blockade of IL-17A function by a neutralizing antibody during ICI treatment significantly reduced ICI-associated thyroid autoimmune infiltrates while preserving the anti-tumor efficacy of anti-PD-1 + anti-CTLA-4 therapy.

DISCUSSION

Immune checkpoint inhibitors (anti-PD-1/L1 and anti-CTLA-4) have significantly advanced the treatment of cancer since their first approval in 2011. However, the benefits and use of ICI have been limited by the frequent development of unwanted IrAEs that contribute to patient morbidity and may lead to interruption of cancer treatment. Current guidelines recommend suspension immunotherapy and high dose glucocorticoid therapy for severe manifestations (grade 3 or 4) of most IrAEs(69, 76), which may unnecessarily impair the efficacy of ICI cancer treatment for many patients(5, 34). Despite significant efforts to date, strategies to reduce IrAEs while supporting ICI-anti-cancer immune responses have been elusive. Using a novel mouse model in which checkpoint inhibitor therapy leads to multi-organ autoimmune infiltrates, we identify Type 3 immune cells, including γδT17 and Th17 cells, as critical contributors to thyroid IrAE development. Antibody-based inhibition of IL-17A protected mice from ICI-induced thyroid autoimmune infiltrates without reducing ICI anti-tumor efficacy. Thus, targeting the IL-17A Type 3 immune axis in ICI-treated patients may be a translatable strategy to reduce IrAEs without impairing the anti-tumor efficacy of ICI.

In our model, ICI-treated NOD mice developed thyroiditis comprised of a T cell predominant but diverse immune infiltrate. Angell *et al.* first reported on the thyroid immune cell infiltrate in a patient with ICI-associated thyroiditis, noting lymphocytic cells and histiocytes(16). In a subsequent study, Kotwal *et al.*(15) evaluated immune cells in thyroid FNA specimens from eight ICI-associated thyroiditis patients and noted a predominant $CD3^+$ T cell population, as well as myeloid cells. Thyroid immune infiltrates in our model are consistent with these data from patients. Finally, a recent report by Yasuda *et al.*(14) evaluating anti-PD-1 therapy in mice pre-immunized with human thyroglobulin, without a tumor, showed a key role for $CD4^+$ T cells in the development of ICI-associated thyroiditis. We further demonstrate the importance of Th17 subsets within $CD4^+$ T cells and highlight the contributions of other T cell populations.

Our data show a role for multiple populations of Type 3 immune cells in the development of thyroid IrAEs, including γδT17, $CD4^+$ Th17, and $CD8^+$ Tc17 cells. We evaluated ICI-associated thyroid immune infiltrates in tumor-free and tumor-bearing mice. These conditions reflect two clinically relevant situations: patients are eligible for ICI treatment in the adjuvant setting with little to no tumor burden, and for primary treatment of metastatic and unresectable tumors with significant tumor burden. Interestingly, γδT17 cells were the primary $IL\text{-}17A^+$ subset in ICI-treated tumor-free mice, but Th17 and Tc17 cells were increased in ICI-treated tumor bearing mice. This may reflect greater activation of the adaptive immune system when a cancer is present due to tumor-derived immune factors. While Th17 cells are well described in spontaneous autoimmunity, including Hashimoto's thyroiditis(19–21), they have not previously been reported in IrAEs. γδT17 cells, in contrast, have not previously been described in studies of spontaneous thyroiditis or in IrAEs(77). γδT17 cells are unique in their early activation and robust cytokine production compared to αβ TCR T cells(55, 78, 79). In addition, γδT17 cells have been reported to expand Th17 cells, and thus early γδT17 activation may contribute to activation and recruitment of Th17, $CD8^+$, and other T cell populations. Future studies can explore the role of γδT17 cells in spontaneous and ICI-induced thyroiditis. Finally, while $CD3^+$ T cells were the primary $IL\text{-}17A^+$ population seen in thyroid immune infiltrates here, production of $IL\text{-}17A^+$ by ILC and myeloid cells may also contribute to IrAEs. Given the multiple arms of Type 3 immunity that may be activated by ICI treatment, inhibition of the common IL-17A axis may prove an effective strategy for the prevention of thyroid IrAEs. Future studies in of thyroid-infiltrating immune cells in patients with thyroid IrAE may further elucidate the role of these cells in human thyroid autoimmunity.

While our study focused on thyroid IrAEs, a common autoimmune side effect encountered during ICI treatment that results in permanent organ dysfunction, these mechanisms may be shared among IrAEs in other organs with more grave clinical consequences. Mice in our model developed multi-organ autoimmunity, including colitis, pneumonitis, hepatitis, and nephritis, and therefore can be used to study IrAEs in these organs. Neutralizing IL-17A antibody therapy decreased overall autoimmune infiltrates, including in non-thyroid tissues (Fig. 4b), and therefore may be of utility in reducing IrAEs during ICI more broadly. ICI-associated colitis has been associated with increased circulating IL-17A in patients treated with anti-CTLA-4 (80, 81) and IL-17 has previously been shown to contribute to spontaneous gut autoimmune diseases, including inflammatory bowel disease(51). $IL\text{-}17A^+$

T cells were prevalent in the colon of NOD mice and colon autoimmune infiltrates were reduced with a neutralizing IL-17A antibody. By comparison, inhibition of IL-17A did not reduce ICI-associated autoimmune diabetes mellitus in this model, emphasizing the importance of tissue-specific immune tolerance mechanisms. Future studies into the role of the IL-17A axis in ICI-associated IrAEs in the colon and other organs are warranted and are facilitated by this new mouse model.

As seen in humans, mice with a genetic predisposition (*i.e.* NOD *vs.* B6) developed more IrAE across multiple tissues following ICI treatment and with combination *vs.* single agent ICI therapy(37, 41). The IrAE predisposition of the inbred NOD strain may also mimic humans with genetic predisposition to IrAE development. Autoimmune predisposition has been mapped to NOD polymorphic regions which include MHC. In humans, the HLADR15 haplotype has been associated with pituitary IrAE(38), HLADR4 with autoimmune diabetes IrAE(37), and HLA-DQB1*03:01 with gut IrAE(39). This model using NOD mice also overcomes some critical limitations of previous models that required deletion of regulatory populations, transfection of human checkpoint proteins, or the requirement for chemical stimulants or xeno-antigen immunization to elicit autoimmunity(14, 31–33, 50). For instance, NOD.H2h4 mice, which have been used previously to study thyroiditis(19, 82, 83) and anti-CTLA-4 induced thyroiditis(33), require excess dietary NaI to precipitate thyroiditis via follicular cell injury and TNFα stimulation, have high background rates of thyroiditis (100% after 6 weeks of NaI supplementation(82)), and require the presence of a non-syngeneic MHC class II molecule(82, 84). In contrast, our model in NOD mice provides an immune competent system with low rates of spontaneous autoimmunity at advanced age, more similar to the background human population. The background incidence of spontaneous thyroiditis of approximately 14% at 1 year in NOD mice(43) compares to a prevalence of near 10% for underlying thyroid autoimmunity in the general population(85–87).

IrAEs remain a significant barrier to the use of ICI but therapeutic strategies to prevent IrAEs have not been widely implemented. A primary consideration in the development of strategies to reduce IrAEs must be the preservation of anti-cancer effects of ICI. As shown here, our model can facilitate these studies using the B16 melanoma and MC38 colon B6 tumor models with genetic deletion of β2M. Several syngeneic NOD tumor models are also in active development by us and others. Early efforts using glucocorticoids for IrAE treatment inconsistently reversed autoimmunity or compromised anti-cancer effects(5, 34). Previous studies have shown reduction of thyroid IrAEs by elimination of $CD4^+$ T cells(14), but this is not readily translatable to cancer patients given the importance of $CD4^+$ T cells in cell-mediated immunity(45, 88). Similarly, while $Tbet1^+$ IFNγ-producing T cells are seen in thyroid immune infiltrates and almost certainly contribute to autoimmunity(89), these cells are known to be critical to anti-cancer effects of ICI(59, 90, 91) and therefore cannot feasibly be inhibited for IrAE prevention. Here we provide evidence that IL-17A blockade may be useful for reducing IrAEs without hindering anti-tumor effects, and in this way may be distinct from other potential inhibitor targets previously reported (*e.g.* CD4 T cells, IFNγ). Therapies targeting the IL-17A pathway are already FDA approved for use in patients(62). Based upon these results, we propose that clinical studies evaluating inhibition

of the IL-17A axis for prevention of IrAEs in cancer patients receiving ICI treatment should be pursued.

Supplementary Material

Refer to Web version on PubMed Central for supplementary material.

Grant support:

This work was supported by funding from the American Thyroid Association (THYROIDGRANT2020-0000000169, M.G.L.), National Institutes of Health (K08 DK129829-01, M.G.L.), Aramont Charitable Foundation (M.G.L.), Parker Institute for Cancer Immunotherapy (M.A.S.), and UCLA Translational pathology core laboratory (TPCL). The funding sources had no role in the study design; the collection, analysis, and interpretation of data; or the writing of the report.

References Cited

1. Wei SC, Duffy CR, and Allison JP. 2018. Fundamental mechanisms of immune checkpoint blockade therapy. Cancer Discov. 8: 1069–1086. [PubMed: 30115704]
2. Haslam A, and Prasad V. 2019. Estimation of the Percentage of US Patients With Cancer Who Are Eligible for and Respond to Checkpoint Inhibitor Immunotherapy Drugs. JAMA Netw. open 2: e192535. [PubMed: 31050774]
3. Larkin J, Chiarion-Sileni V, Gonzalez R, Grob JJ, Rutkowski P, Lao CD, Cowey CL, Schadendorf D, Wagstaff J, Dummer R, Ferrucci PF, Smylie M, Hogg D, Hill A, Márquez-Rodas I, Haanen J, Guidoboni M, Maio M, Schöffski P, Carlino MS, Lebbé C, McArthur G, Ascierto PA, Daniels GA, Long GV, Bastholt L, Rizzo JI, Balogh A, Moshyk A, Hodi FS, and Wolchok JD. 2019. Five-year survival with combined nivolumab and ipilimumab in advanced melanoma. N. Engl. J. Med 381: 1535–1546. [PubMed: 31562797]
4. Arnaud-Coffin P, Maillet D, Gan HK, Stelmes JJ, You B, Dalle S, and Péron J. 2019. A systematic review of adverse events in randomized trials assessing immune checkpoint inhibitors. Int. J. Cancer 145: 639–648. [PubMed: 30653255]
5. Das S, and Johnson DB. 2019. Immune-related adverse events and anti-tumor efficacy of immune checkpoint inhibitors. J. Immunother. Cancer 7: 1–11. [PubMed: 30612589]
6. De Filette J, Andreescu CE, Cools F, Bravenboer B, and Velkeniers B. 2019. A Systematic Review and Meta-Analysis of Endocrine-Related Adverse Events Associated with Immune Checkpoint Inhibitors. Horm. Metab. Res 51: 145–156. [PubMed: 30861560]
7. Wang DY, Salem JE, Cohen JV, Chandra S, Menzer C, Ye F, Zhao S, Das S, Beckermann KE, Ha L, Rathmell WK, Ancell KK, Balko JM, Bowman C, Davis EJ, Chism DD, Horn L, Long GV, Carlino MS, Lebrun-Vignes B, Eroglu Z, Hassel JC, Menzies AM, Sosman JA, Sullivan RJ, Moslehi JJ, and Johnson DB. 2018. Fatal Toxic Effects Associated With Immune Checkpoint Inhibitors: A Systematic Review and Meta-analysis. JAMA Oncol. 4: 1721–1728. [PubMed: 30242316]
8. Young A, Quandt Z, and Bluestone JA. 2018. The balancing act between cancer immunity and autoimmunity in response to immunotherapy. Cancer Immunol. Res 6: 1445–1452. [PubMed: 30510057]
9. Iyer PC, Cabanillas ME, Waguespack SG, Hu MI, Thosani S, Lavis VR, Busaidy NL, Subudhi SK, Diab A, and Dadu R. 2018. Immune-Related Thyroiditis with Immune Checkpoint Inhibitors. Thyroid 28: 1243–1251. [PubMed: 30132401]
10. Delivanis DA, Gustafson MP, Bornschlegl S, Merten MM, Kottschade L, Withers S, Dietz AB, and Ryder M. 2017. Pembrolizumab-induced thyroiditis: Comprehensive clinical review and insights into underlying involved mechanisms. J. Clin. Endocrinol. Metab 102: 2770–2780. [PubMed: 28609832]
11. De Moel EC, Rozeman EA, Kapiteijn EH, Verdegaal EME, Grummels A, Bakker JA, Huizinga TWJ, Haanen JB, Toes REM, and Van Der Woude D. 2019. Autoantibody development

under treatment with immune-checkpoint inhibitors. Cancer Immunol. Res 7: 6–11. [PubMed: 30425107]

12. Ma C, Hodi FS, Giobbie-Hurder A, Wang X, Zhou J, Zhang A, Zhou Y, Mao F, Angell TE, Andrews CP, Hu J, Barroso-Sousa R, Kaiser UB, Tolaney SM, and Min L. 2019. The impact of high-dose glucocorticoids on the outcome of immune-checkpoint inhibitor–related thyroid disorders. Cancer Immunol. Res 7: 1214–1220. [PubMed: 31088848]
13. Álvarez-Sierra D, Marín-Sánchez A, Ruiz-Blázquez P, de Jesús Gil C, Iglesias-Felip C, González Ó, Casteras A, Costa RF, Nuciforo P, Colobran R, and Pujol-Borrell R. 2019. Analysis of the PD-1/PD-L1 axis in human autoimmune thyroid disease: Insights into pathogenesis and clues to immunotherapy associated thyroid autoimmunity. J. Autoimmun 103.
14. Yasuda Y, Iwama S, Sugiyama D, Okuji T, Kobayashi T, Ito M, Okada N, Enomoto A, Ito S, Yan Y, Sugiyama M, Onoue T, Tsunekawa T, Ito Y, Takagi H, Hagiwara D, Goto M, Suga H, Banno R, Takahashi M, Nishikawa H, and Arima H. 2021. CD4 + T cells are essential for the development of destructive thyroiditis induced by anti – PD-1 antibody in thyroglobulin-immunized mice. 7495.
15. Kotwal A, Gustafson MP, Bornschlegl S, Kottschade L, Delivanis DA, Dietz AB, Gandhi M, and Ryder M. 2020. Immune Checkpoint Inhibitor-Induced Thyroiditis Is Associated with Increased Intrathyroidal T Lymphocyte Subpopulations. Thyroid 00: 1–11.
16. Angell TE, Min L, Wieczorek TJ, and Hodi FS. 2018. Unique cytologic features of thyroiditis caused by immune checkpoint inhibitor therapy for malignant melanoma. Genes Dis. 5: 46–48. [PubMed: 29619406]
17. Jabkowski J, Loidl A, Auinger B, Kehrer H, Sepp N, and Pichler R. 2021. Pembrolizumab-Induced Thyroiditis Shows PD-L1Expressing Histiocytes and Infiltrating T Cells in Thyroid Tissue - A Case Report. Front. Immunol 12: 10–14.
18. Rydzewska M, Jaromin M, Pasierowska IE, Stozek K, and Bossowski A. 2018. Role of the T and B lymphocytes in pathogenesis of autoimmune thyroid diseases. Thyroid Res. 11: 1–11. [PubMed: 29375671]
19. Horie I, Abiru N, Nagayama Y, Kuriya G, Saitoh O, Ichikawa T, Iwakura Y, and Eguchi K. 2009. T helper type 17 immune response plays an indispensable role for development of iodine-induced autoimmune thyroiditis in nonobese diabetic-H2h4 mice. Endocrinology 150: 5135–5142. [PubMed: 19797122]
20. Konca Degertekin C, Aktas Yilmaz B, Balos Toruner F, Kalkanci A, Turhan Iyidir O, Fidan I, Yesilyurt E, Cakir N, Kustimur S, and Arslan M. 2016. Circulating Th17 cytokine levels are altered in Hashimoto's thyroiditis. Cytokine 80: 13–17. [PubMed: 26928603]
21. Shi Y, Wang H, Su Z, Chen J, Xue Y, Wang S, Xue Y, He Z, Yang H, Zhou C, Kong F, Liu Y, Yang P, Lu L, Shao Q, Huang X, and Xu H. 2010. Differentiation imbalance of Th1/Th17 in peripheral blood mononuclear cells might contribute to pathogenesis of Hashimoto's thyroiditis. Scand. J. Immunol 72: 250–255. [PubMed: 20696023]
22. Su MA, Giang K, Žumer K, Jiang H, Oven I, Rinn JL, DeVoss JJ, Johannes KPA, Lu W, Gardner J, Chang A, Bubulya P, Chang HY, Peterlin BM, and Anderson MS. 2008. Mechanisms of an autoimmunity syndrome in mice caused by a dominant mutation in Aire. J. Clin. Invest 118: 1712–1726. [PubMed: 18414681]
23. Torrejon DY, Abril-Rodriguez G, Champhekar AS, Tsoi J, Campbell KM, Kalbasi A, Parisi G, Zaretsky JM, Garcia-Diaz A, Puig-Saus C, Cheung-Lau G, Wohlwender T, Krystofinski P, Vega-Crespo A, Lee CM, Mascaro P, Grasso CS, Berent-Maoz B, Comin-Anduix B, Hu-Lieskovan S, and Ribas A. 2020. Overcoming Genetically Based Resistance Mechanisms to PD-1 Blockade. Cancer Discov. 10: 1140 LP – 1157. [PubMed: 32467343]
24. Ostanin DV, Pavlick KP, Bharwani S, D'Souza D, Furr KL, Brown CM, and Grisham MB. 2006. T cell-induced inflammation of the small and large intestine in immunodeficient mice. Am. J. Physiol. Gastrointest. Liver Physiol 290: G109–19. [PubMed: 16099868]
25. Moreno BH, Zaretsky JM, Garcia-Diaz A, Tsoi J, Parisi G, Robert L, Meeth K, Ndoye A, Bosenberg M, Weeraratna AT, Graeber TG, Comin-Anduix B, Hu-Lieskovan S, and Ribas A. 2016. Response to programmed cell death-1 blockade in a murine melanoma syngeneic model requires costimulation, CD4, and CD8 T cells. Cancer Immunol. Res 4: 845–857. [PubMed: 27589875]

26. Terszowski G, Müller SM, Bleul CC, Blum C, Schirmbeck R, Reimann J, Du Pasquier L, Amagai T, Boehm T, and Rodewald H-R. 2006. Evidence for a functional second thymus in mice. Science 312: 284–287. [PubMed: 16513945]
27. Stuart T, Butler A, Hoffman P, Hafemeister C, Papalexi E, Mauck WM, Hao Y, Stoeckius M, Smibert P, and Satija R. 2019. Comprehensive Integration of Single-Cell Data. Cell 177: 1888–1902.e21. [PubMed: 31178118]
28. Tirosh I, Izar B, Prakadan SM, Wadsworth MH, Treacy D, Trombetta JJ, Rotem A, Rodman C, Lian C, Murphy G, Fallahi-Sichani M, Dutton-Regester K, Lin JR, Cohen O, Shah P, Lu D, Genshaft AS, Hughes TK, Ziegler CGK, Kazer SW, Gaillard A, Kolb KE, Villani AC, Johannessen CM, Andreev AY, Van Allen EM, Bertagnolli M, Sorger PK, Sullivan RJ, Flaherty KT, Frederick DT, Jané-Valbuena J, Yoon CH, Rozenblatt-Rosen O, Shalek AK, Regev A, and Garraway LA. 2016. Dissecting the multicellular ecosystem of metastatic melanoma by single-cell RNA-seq. Science (80–.). 352: 189–196.
29. Chen EY, Tan CM, Kou Y, Duan Q, Wang Z, Meirelles GV, Clark NR, and Ma'ayan A. 2013. Enrichr: interactive and collaborative HTML5 gene list enrichment analysis tool. BMC Bioinformatics 14: 128. [PubMed: 23586463]
30. Heng TSP, and Painter MW. 2008. The Immunological Genome Project: networks of gene expression in immune cells. Nat. Immunol 9: 1091–1094. [PubMed: 18800157]
31. Liu J, Blake SJ, Harjunpää H, Fairfax KA, Yong MCR, Allen S, Kohrt HE, Takeda K, Smyth MJ, and Teng MWL. 2016. Assessing immune-related adverse events of efficacious combination immunotherapies in preclinical models of cancer. Cancer Res. 76: 5288–5301. [PubMed: 27503925]
32. Du X, Liu M, Su J, Zhang P, Tang F, Ye P, Devenport M, Wang X, Zhang Y, Liu Y, and Zheng P. 2018. Uncoupling therapeutic from immunotherapy-related adverse effects for safer and effective anti-CTLA-4 antibodies in CTLA4 humanized mice. Cell Res. 28: 433–447. [PubMed: 29463898]
33. Sharma R, Di Dalmazi G, and Caturegli P. 2016. Exacerbation of Autoimmune Thyroiditis by CTLA-4 Blockade: A Role for IFNγ-Induced Indoleamine 2, 3-Dioxygenase. Thyroid 26: 1117–1124. [PubMed: 27296629]
34. Adam K, Iuga A, Tocheva AS, and Mor A. 2021. A novel mouse model for checkpoint inhibitor-induced adverse events. PLoS One 16: 1–14.
35. Toi Y, Sugawara S, Sugisaka J, Ono H, Kawashima Y, Aiba T, Kawana S, Saito R, Aso M, Tsurumi K, Suzuki K, Shimizu H, Domeki Y, Terayama K, Nakamura A, Yamanda S, Kimura Y, and Honda Y. 2019. Profiling Preexisting Antibodies in Patients Treated with Anti-PD-1 Therapy for Advanced Non-Small Cell Lung Cancer. JAMA Oncol. 5: 376–383. [PubMed: 30589930]
36. Nakamura Y 2019. Biomarkers for Immune Checkpoint Inhibitor-Mediated Tumor Response and Adverse Events. Front. Med 6.
37. Bluestone JA, Anderson M, Herold KC, Stamatouli AM, Quandt Z, Perdigoto AL, Clark PL, Kluger H, Weiss SA, Gettinger S, Sznol M, Young A, Rushakoff R, and Lee J. 2018. Collateral damage: Insulin-dependent diabetes induced with checkpoint inhibitors. In Diabetes vol. 67. American Diabetes Association Inc. 1471–1480. [PubMed: 29937434]
38. Yano S, Ashida K, Sakamoto R, Sakaguchi C, Ogata M, Maruyama K, Sakamoto S, Ikeda M, Ohe K, Akasu S, Iwata S, Wada N, Matsuda Y, Nakanishi Y, Nomura M, and Ogawa Y. 2020. Human leucocyte antigen DR15, a possible predictive marker for immune checkpoint inhibitor–induced secondary adrenal insufficiency. Eur. J. Cancer 130: 198–203. [PubMed: 32229416]
39. Hasan Ali O, Berner F, Bomze D, Fässler M, Diem S, Cozzio A, Jörger M, Früh M, Driessen C, Lenz TL, and Flatz L. 2019. Human leukocyte antigen variation is associated with adverse events of checkpoint inhibitors. Eur. J. Cancer 107: 8–14. [PubMed: 30529903]
40. Khan Z, Di Nucci F, Kwan A, Hammer C, Mariathasan S, Rouilly V, Carroll J, Fontes M, Acosta SL, Guardino E, Chen-Harris H, Bhangale T, Mellman I, Rosenberg J, Powles T, Hunkapiller J, Chandler GS, and Albert ML. 2020. Polygenic risk for skin autoimmunity impacts immune checkpoint blockade in bladder cancer. Proc. Natl. Acad. Sci. U. S. A 117: 12288–12294. [PubMed: 32430334]
41. Yamazaki H, Iwasaki H, Yamashita T, Yoshida T, Suganuma N, Yamanaka T, Masudo K, Nakayama H, Kohagura K, Rino Y, and Masuda M. 2017. Potential risk factors for nivolumab-induced thyroid dysfunction. In Vivo (Brooklyn). 31: 1225–1228.

42. Podolin PL, Pressey A, DeLarato NH, Fischer PA, Peterson LB, and Wicker LS. 1993. I-E+ nonobese diabetic mice develop insulitis and diabetes. J. Exp. Med 178: 793–804. [PubMed: 8350054]
43. Damotte D, Colomb E, Cailleau C, Brousse N, Charreire J, and Carnaud C. 1997. Analysis of susceptibility of NOD mice to spontaneous and experimentally induced thyroiditis. Eur. J. Immunol 27: 2854–2862. [PubMed: 9394810]
44. Anderson MS, and Bluestone JA. 2005. THE NOD MOUSE: A Model of Immune Dysregulation. Annu. Rev. Immunol 23: 447–485. [PubMed: 15771578]
45. Oh DY, Kwek SS, Raju SS, Li T, McCarthy E, Chow E, Aran D, Ilano A, Pai CCS, Rancan C, Allaire K, Burra A, Sun Y, Spitzer MH, Mangul S, Porten S, Meng MV, Friedlander TW, Ye CJ, and Fong L. 2020. Intratumoral CD4+ T Cells Mediate Anti-tumor Cytotoxicity in Human Bladder Cancer. Cell 181: 1612–1625.e13. [PubMed: 32497499]
46. Yost KE, Satpathy AT, Wells DK, Qi Y, Kageyama R, Mcnamara K, Granja JM, Sarin KY, Brown RA, Gupta RK, Curtis C, and Bucktrout SL. 2020. Clonal replacement of tumor-specific T cells following PD-1 blockade. 25: 1251–1259.
47. Postow MA, Sidlow R, and Hellmann MD. 2018. Immune-related adverse events associated with immune checkpoint blockade. N. Engl. J. Med 378: 158–168. [PubMed: 29320654]
48. Quintana FJ, and Cohen IR. 2001. Autoantibody patterns in diabetes-prone NOD mice and in standard C57BL/6 mice. J. Autoimmun 17: 191–197. [PubMed: 11712856]
49. Jiang W, Anderson MS, Bronson R, Mathis D, and Benoist C. 2005. Modifier loci condition autoimmunity provoked by Aire deficiency. J. Exp. Med 202: 805–815. [PubMed: 16172259]
50. Perez-Ruiz E, Minute L, Otano I, Alvarez M, Ochoa MC, Belsue V, de Andrea C, Rodriguez-Ruiz ME, Perez-Gracia JL, Marquez-Rodas I, Llacer C, Alvarez M, de Luque V, Molina C, Teijeira A, Berraondo P, and Melero I. 2019. Prophylactic TNF blockade uncouples efficacy and toxicity in dual CTLA-4 and PD-1 immunotherapy. Nature 569: 428–432. [PubMed: 31043740]
51. Miossec P, Korn T, and Kuchroo VK. 2009. Interleukin-17 and type 17 helper T cells. N. Engl. J. Med 361: 888. [PubMed: 19710487]
52. Barros-Martins J, Schmolka N, Fontinha D, Pires de Miranda M, Simas JP, Brok I, Ferreira C, Veldhoen M, Silva-Santos B, and Serre K. 2016. Effector γδ T Cell Differentiation Relies on Master but Not Auxiliary Th Cell Transcription Factors. J. Immunol 196: 3642–3652. [PubMed: 26994218]
53. Ivanov II, McKenzie BS, Zhou L, Tadokoro CE, Lepelley A, Lafaille JJ, Cua DJ, and Littman DR. 2006. The orphan nuclear receptor RORgammat directs the differentiation program of proinflammatory IL-17+ T helper cells. Cell 126: 1121–1133. [PubMed: 16990136]
54. Tang C, Chen S, Qian H, and Huang W. 2012. Interleukin-23: As a drug target for autoimmune inflammatory diseases. Immunology 135: 112–124. [PubMed: 22044352]
55. Papotto PH, Reinhardt A, Prinz I, and Silva-Santos B. 2018. Innately versatile: γδ17 T cells in inflammatory and autoimmune diseases. J. Autoimmun 87: 26–37. [PubMed: 29203226]
56. Liang Y, Pan HF, and Ye DQ. 2015. Tc17 cells in immunity and systemic autoimmunity. Int. Rev. Immunol 34: 318–331. [PubMed: 25259411]
57. Kuen DS, Kim BS, and Chung Y. 2020. Il-17-producing cells in tumor immunity: Friends or foes? Immune Netw. 20: 1–20.
58. Mancini M, Vergara E, Salvatore G, Greco A, Troncone G, Affuso A, Liuzzi R, Salerno P, Scotto di Santolo M, Santoro M, Brunetti A, and Salvatore M. 2009. Morphological Ultrasound Microimaging of Thyroid in Living Mice. Endocrinology 150: 4810–4815. [PubMed: 19589864]
59. Ayers M, Lunceford J, Nebozhyn M, Murphy E, Loboda A, Kaufman DR, Albright A, Cheng JD, Kang SP, Shankaran V, Piha-Paul SA, Yearley J, Seiwert TY, Ribas A, and McClanahan TK. 2017. IFN-γ-related mRNA profile predicts clinical response to PD-1 blockade. J. Clin. Invest 127: 2930–2940. [PubMed: 28650338]
60. Oh DY, Cham J, Zhang L, Fong G, Kwek SS, Klinger M, Faham M, and Fong L. 2017. Immune toxicities elicted by CTLA-4 blockade in cancer patients are associated with early diversification of the T-cell repertoire. Cancer Res. 77: 1322–1330. [PubMed: 28031229]
61. Tan L, Sandrock I, Odak I, Aizenbud Y, Wilharm A, Barros-Martins J, Tabib Y, Borchers A, Amado T, Gangoda L, Herold MJ, Schmidt-Supprian M, Kisielow J, Silva-Santos B, Koenecke

C, Hovav AH, Krebs C, Prinz I, and Ravens S. 2019. Single-Cell Transcriptomics Identifies the Adaptation of Scart1+ Vγ6+ T Cells to Skin Residency as Activated Effector Cells. Cell Rep. 27: 3657–3671.e4. [PubMed: 31216482]

62. Miossec P 2021. Local and systemic effects of IL-17 in joint inflammation: a historical perspective from discovery to targeting. Cell. Mol. Immunol 18: 860–865. [PubMed: 33692481]
63. Veldhoen M, Hocking RJ, Atkins CJ, Locksley RM, and Stockinger B. 2006. TGFβ in the context of an inflammatory cytokine milieu supports de novo differentiation of IL-17-producing T cells. Immunity 24: 179–189. [PubMed: 16473830]
64. Badran YR, Cohen JV, Brastianos PK, Parikh AR, Hong TS, and Dougan M. 2019. Concurrent therapy with immune checkpoint inhibitors and TNFα blockade in patients with gastrointestinal immune-related adverse events. J. Immunother. Cancer 7.
65. Kang JH, Bluestone JA, and Young A. 2021. Predicting and Preventing Immune Checkpoint Inhibitor Toxicity: Targeting Cytokines. Trends Immunol. 42: 293–311. [PubMed: 33714688]
66. Young A, Nguyen V, Mehdizadeh S, Sheehan KCF, V Serreze D, Schreiber RD, and Bluestone JA. 2018. Development of syngeneic NOD tumor models to study tumor immunity in autoimmune-prone mice,.
67. Stewart TJ, and Abrams SI. 2008. How tumours escape mass destruction. Oncogene 27: 5894–5903. [PubMed: 18836470]
68. Angell TE, Lechner MG, Jang JK, LoPresti JS, and Epstein AL. 2014. MHC class I loss is a frequent mechanism of immune escape in papillary thyroid cancer that is reversed by interferon and selumetinib treatment in Vitro. Clin. Cancer Res 20: 6034–6044. [PubMed: 25294906]
69. Thompson JA, Schneider BJ, Brahmer J, Achufusi A, Armand P, Berkenstock MK, Bhatia S, Budde LE, Chokshi S, Davies M, Elshoury A, Gesthalter Y, Hegde A, Jain M, Kaffenberger BH, Lechner MG, Li T, Marr A, McGettigan S, McPherson J, Medina T, Mohindra NA, Olszanski AJ, Oluwole O, Patel SP, Patil P, Reddy S, Ryder M, Santomasso B, Shofer S, Sosman JA, Wang Y, Zaha VG, Lyons M, Dwyer M, and Hang L. 2022. Management of Immunotherapy-Related Toxicities, Version 1.2022, NCCN Clinical Practice Guidelines in Oncology. J. Natl. Compr. Cancer Netw 20: 387–405.
70. Xing P, Zhang F, Wang G, Xu Y, Li C, Wang S, Guo Y, Cai S, Wang Y, and Li J. 2019. Incidence rates of immune-related adverse events and their correlation with response in advanced solid tumours treated with NIVO or NIVO+IPI: A systematic review and meta-analysis. J. Immunother. Cancer 7.
71. Cheung Y-MM, Wang W, McGregor B, and Hamnvik O-PR. 2022. Associations between immune-related thyroid dysfunction and efficacy of immune checkpoint inhibitors: a systematic review and meta-analysis. Cancer Immunol. Immunother.
72. Kotwal A, Kottschade L, and Ryder M. 2020. PD-L1 Inhibitor-Induced Thyroiditis Is Associated with Better Overall Survival in Cancer Patients. Thyroid 30: 1–8. [PubMed: 31842720]
73. Fabre J, Giustiniani J, Garbar C, Antonicelli F, Merrouche Y, Bensussan A, Bagot M, and Al-Dacak R. 2016. Targeting the tumor microenvironment: The protumor effects of IL-17 related to cancer type. Int. J. Mol. Sci 17.
74. Zhao J, Chen X, Herjan T, and Li X. 2020. The role of interleukin-17 in tumor development and progression. J. Exp. Med 217: 1–13.
75. Liu C, Liu R, Wang B, Lian J, Yao Y, Sun H, Zhang C, Fang L, Guan X, Shi J, Han S, Zhan F, Luo S, Yao Y, Zheng T, and Zhang Y. 2021. Blocking IL-17A enhances tumor response to anti-PD-1 immunotherapy in microsatellite stable colorectal cancer. J. Immunother. cancer 9.
76. Brahmer JR, Lacchetti C, Schneider BJ, Atkins MB, Brassil KJ, Caterino JM, Chau I, Ernstoff MS, Gardner JM, Ginex P, Hallmeyer S, Chakrabarty JH, Leighl NB, Mammen JS, Mcdermott DF, Naing A, Nastoupil LJ, Phillips T, Porter LD, Puzanov I, Reichner CA, Santomasso BD, Seigel C, Spira A, Suarez-Almazor ME, Wang Y, Weber JS, Wolchok JD, and Thompson JA. 2018. JOURNAL OF CLINICAL ONCOLOGY. J Clin Oncol 36: 1714–1768. [PubMed: 29442540]
77. Paolieri F, Pronzato C, Battifora M, Fiorino N, Canonica GW, and Bagnasco M. 1995. Infiltrating γ/gd T-cell receptor-positive lymphocytes in Hashimoto's thyroiditis, Graves' disease and papillary thyroid cancer. J. Endocrinol. Invest 18: 295–298. [PubMed: 7560812]

78. Papotto PH, Ribot JC, and Silva-Santos B. 2017. IL-17 + γδ T cells as kick-starters of inflammation. Nat. Immunol 18: 604–611. [PubMed: 28518154]

79. Sutton CE, Lalor SJ, Sweeney CM, Brereton CF, Lavelle EC, and Mills KHG. 2009. Interleukin-1 and IL-23 Induce Innate IL-17 Production from γδ T Cells, Amplifying Th17 Responses and Autoimmunity. Immunity 31: 331–341. [PubMed: 19682929]

80. Tarhini AA, Zahoor H, Lin Y, Malhotra U, Sander C, Butterfield LH, and Kirkwood JM. 2015. Baseline circulating IL-17 predicts toxicity while TGF-β1 and IL-10 are prognostic of relapse in ipilimumab neoadjuvant therapy of melanoma. J. Immunother. Cancer 3: 15–20. [PubMed: 25901287]

81. von Euw E, Chodon T, Attar N, Jalil J, Koya RC, Comin-Anduix B, and Ribas A. 2009. CTLA4 blockade increases Th17 cells in patients with metastatic melanoma. J. Transl. Med 7: 1–13. [PubMed: 19123955]

82. Braley-Mullen H, Sharp GC, Medling B, and Tang H. 1999. Spontaneous Autoimmune Thyroiditis in NOD.H-2h4 Mice,.

83. McLachlan SM, Aliesky HA, and Rapoport B. 2018. Aberrant Iodine Autoregulation Induces Hypothyroidism in a Mouse Strain in the Absence of Thyroid Autoimmunity. J. Endocr. Soc 2: 63–76. [PubMed: 29379895]

84. McLachlan SM, Lesage S, Collin R, Banuelos B, Aliesky HA, and Rapoport B. 2017. Genes outside the major histocompatibility complex locus are linked to the development of thyroid autoantibodies and thyroiditis in NOD.H2h4 mice. Endocrinology 158: 702–713. [PubMed: 28323998]

85. O'Leary PC, Feddema PH, Michelangeli VP, Leedman PJ, Chew GT, Knuiman M, Kaye J, and Walsh JP. 2006. Investigations of thyroid hormones and antibodies based on a community health survey: The Busselton thyroid study. Clin. Endocrinol. (Oxf). 64: 97–104. [PubMed: 16402936]

86. Tunbridge WMG, Evered DC, Hall R, Appleton D, Brewis M, Clark F, Evans JG, Young E, Bird T, And Smith PA. 1977. The Spectrum Of Thyroid Disease In A Community: The Whickham Survey. Clin. Endocrinol. (Oxf). 7: 481–493. [PubMed: 598014]

87. Hollowell JG, Staehling NW, Flanders WD, Hannon WH, Gunter EW, Spencer CA, and Braverman LE. 2002. Serum TSH, T(4), and thyroid antibodies in the United States population (1988 to 1994): National Health and Nutrition Examination Survey (NHANES III). J. Clin. Endocrinol. Metab 87: 489–499. [PubMed: 11836274]

88. Tay RE, Richardson EK, and Toh HC. 2021. Revisiting the role of CD4+ T cells in cancer immunotherapy—new insights into old paradigms. Cancer Gene Ther. 28: 5–17. [PubMed: 32457487]

89. Horie I, Abiru N, Sakamoto H, Iwakura Y, and Nagayama Y. 2011. Induction of autoimmune thyroiditis by depletion of CD4 +CD25 + regulatory T cells in thyroiditis-resistant IL-17, but not interferon-γ receptor, knockout nonobese diabetic-H2 h4 mice. Endocrinology 152: 4448–4454. [PubMed: 21862617]

90. Gao J, Shi LZ, Zhao H, Chen J, Xiong L, He Q, Chen T, Roszik J, Bernatchez C, Woodman SE, Chen PL, Hwu P, Allison JP, Futreal A, Wargo JA, and Sharma P. 2016. Loss of IFN-γ Pathway Genes in Tumor Cells as a Mechanism of Resistance to Anti-CTLA-4 Therapy. Cell 167: 397–404.e9. [PubMed: 27667683]

91. Shi LZ, Fu T, Guan B, Chen J, Blando JM, Allison JP, Xiong L, Subudhi SK, Gao J, and Sharma P. 2016. Interdependent IL-7 and IFN-γ signalling in T-cell controls tumour eradication by combined α-CTLA-4+α-PD-1 therapy. Nat. Commun 7.

Key points:

Tumor-bearing NOD mice model immune checkpoint inhibitor-associated autoimmunity.

γδT17 and Th17 type 3 immune cells contribute to ICI-associated thyroiditis.

IL-17A inhibition reduces thyroid autoimmunity but preserves ICI anti-tumor response.

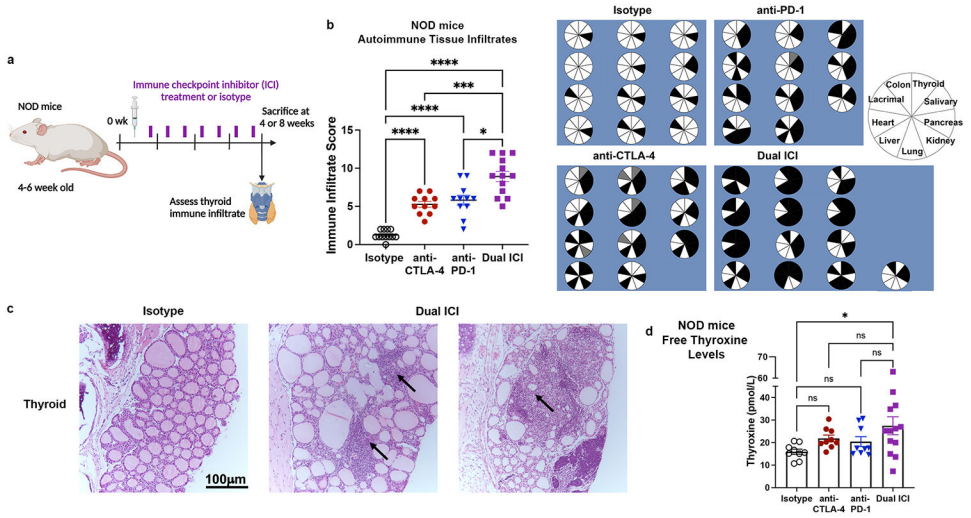

Figure 1. ICI therapy induces multi-system autoimmune infiltrates (IrAE) in NOD mice.

a, Schematic of ICI drug treatment. **b**, Comparison of autoimmune organ infiltration and severity by immune infiltrate score after 8 weeks of ICI treatment in NOD mice [n=12 isotype, n=11 anti-CTLA-4, n=11 anti-PD-1, and n=13 Dual ICI (anti-PD-1 + anti-CTLA-4)]. Pie charts show tissue infiltrate for each mouse; black = immune infiltrate, white = no infiltrate, gray = no data. **c**, Representative H&E micrographs of thyroid autoimmune tissue infiltrates in isotype (*left*) *vs.* Dual ICI (*right*) treated mice (original mag. 400x). Arrows indicate areas of focal infiltrates. **d**, Free thyroxine serum levels in ICI-treated NOD mice after 8 weeks of treatment. Data are mean±SEM. *p<0.05, ***p<0.001, ****p<0.0001, Brown-Forsythe ANOVA, assuming unequal s.d., followed by Dunnett's multiple comparisons test (**b**), or one-way ANOVA and Dunnett's multiple comparison test (**d**).

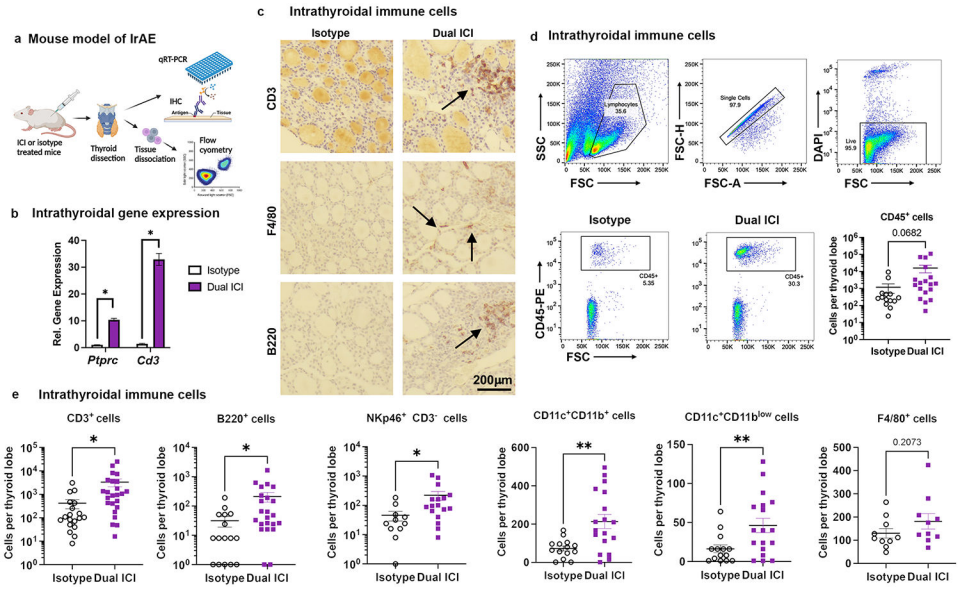

Figure 2. Characterization of thyroid-infiltrating immune cells in ICI-treated NOD mice.

a, Schematic of thyroid immune cell infiltrate evaluation in ICI-treated NOD mice. **b,** Comparison of intrathyroidal gene expression in isotype *vs.* Dual ICI-treated mice for lineage genes *ptprc* and *Cd3e* measured by qRT-PCR. n=12 animals/group; thyroid tissue pooled and run in 3 experiments, in triplicate. **c**, IHC staining for T cells (CD3), macrophages (F4/80), and B cells (B220) in thyroid tissue from isotype or Dual ICI-treated mice (representative sections, 400x original mag.) **d-e**, Comparison of thyroid immune cell infiltrate by flow cytometry. Representative gating strategies and dot plots and comparison of accumulated $CD45^+$ immune cells (**c**) and subpopulations (**d**) in thyroid tissue from isotype (n=11, except n=16 for $CD3^+$ and $B220^+$) *vs.* Dual ICI-treated (n=17, except n=23 for $CD3^+$ and $B220^+$) mice after 4 weeks. Data shown as absolute cells per thyroid lobe. Data are mean±SEM. *p<0.05, **p<0.01, two-tailed, unpaired t test with Welch correction, assuming unequal s.d. and Holm-Sidak method correction for multiple comparisons (**b, d-e**).

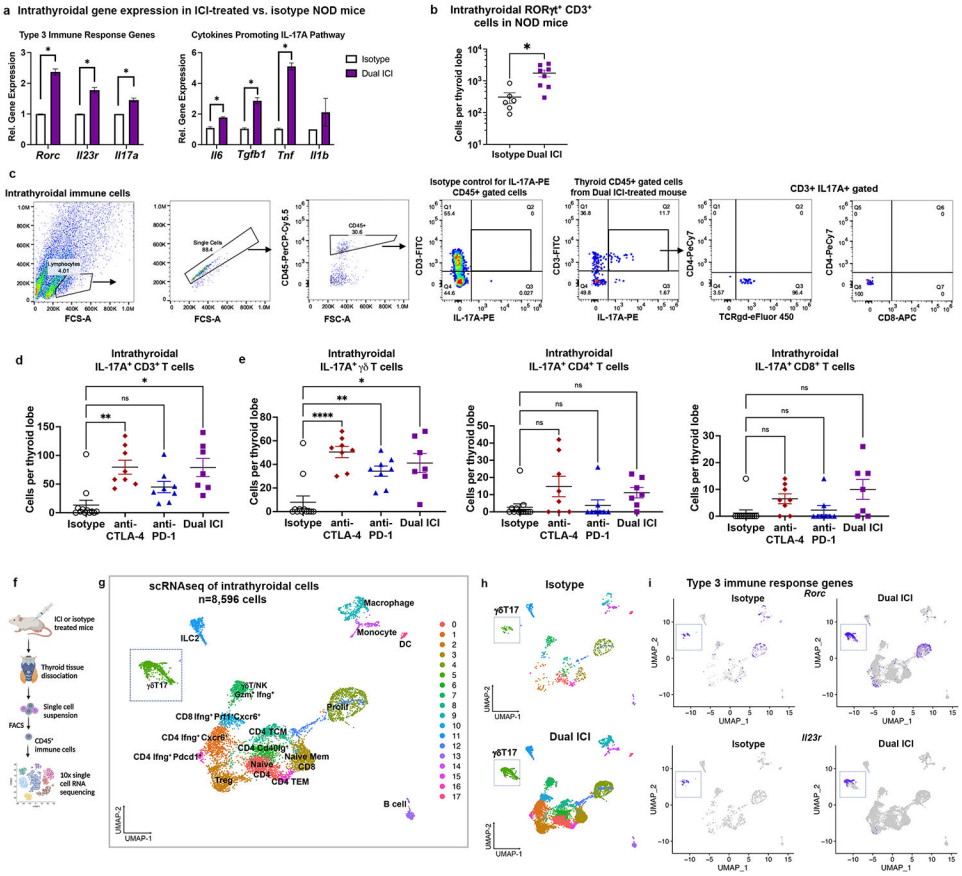

Figure 3. RORγt$^+$ IL-17A$^+$ T cells in thyroid immune infiltrates of ICI-treated mice.

a, Comparison of intrathyroidal gene expression in isotype *vs.* Dual ICI-treated mice for Type 3 immunity (RORγt-pathway) associated genes *Rorc, Il23r, Il17a,* and cytokines associated with IL-17A pathway differentiation (*IL6, Tgfb1, Tnf, Il1b)* measured by qRT-PCR. n=12 animals/group; thyroid tissue pooled and run in 3 experiments, in triplicate. **b**, Comparison of thyroid-infiltrating RORγt$^+$ CD3$^+$ (αβ and γδ) T cells by flow cytometry in isotype (n=6) *vs.* Dual ICI-treated (n=8) mice. **c**, Representative flow cytometry plots and gating strategy and quantification of intrathyroidal IL-17A$^+$ CD3$^+$ T cells (**d**) and IL-17A$^+$ T cell subsets (**e**) from ICI-treated mice at 4 weeks; isotype (n=12), anti-PD-1 (n=8), anti-CTLA-4 (n=8), and Dual ICI (n=7). Data are mean ±SEM shown. **f,** Schematic of thyroid tissue processing for scRNAseq from Dual ICI or isotype-treated mice. **g,** UMAP plot of thyroid-infiltrating CD45$^+$ immune cells from Dual ICI-treated (n=16) or isotype-treated (n=10) mice. Cluster analysis yields 18 distinct clusters comprising CD4, CD8, and γδ T cells, natural killer (NK) cells, innate lymphoid cells type 2 (ILC2), B cells, macrophages, monocytes, dendritic cells (DC), as well as clusters with mixed cell populations clustered by markers of cell proliferation (prolif). T effector memory, TEM. T central memory, TCM. T regulatory cells, Treg. **h,** Split plot showing distribution of cells by condition. **i,** Feature plots showing *Rorc*$^+$ and *Il23r*$^+$ cells associated primarily with γδ T cell clusters in intrathyroidal immune cells from isotype or ICI-treated NOD mice by scRNAseq. *p<0.05, **p<0.01, ***p<0.001, ****p<0.0001. two-tailed, unpaired t test with Welch correction, assuming unequal s.d. (**a, b**) and Holm-Sidak method correction for multiple comparisons (**a**); Brown-

Forsythe ANOVA, assuming unequal s.d., followed by Dunnett's multiple comparisons test (**d-e**).

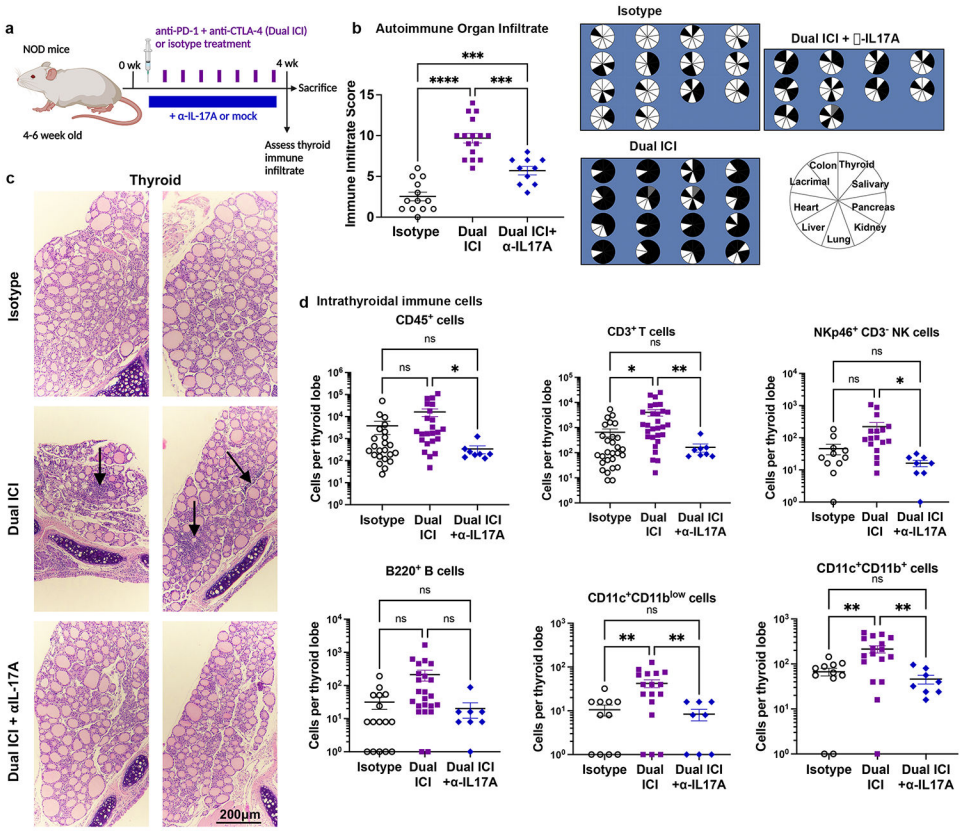

Figure 4. Neutralizing interleukin (IL)-17A antibody therapy reduces ICI-associated thyroid autoimmune infiltrates.

a, Schematic of treatment regimen combining anti-PD-1 + anti-CTLA-4 (Dual ICI) with a neutralizing IL-17A antibody (αIL-17A) in NOD mice. **b**, Autoimmune organ infiltrate score after 4 weeks of ICI treatment in isotype (*n*=14), Dual ICI (*n*=16), or Dual ICI + αIL-17A (*n*=10). Pie charts (*right*) showing tissues with immune infiltration after 4 weeks of ICI treatment. Each pie represents one animal; black = immune infiltrate, white = no infiltrate, gray = no data. **c,** Representative H&E micrographs of thyroid immune infiltrates in isotype (*top*), Dual ICI (*middle*), or Dual ICI + αIL-17A (*bottom*) treated mice (original mag. 400x). Arrows indicate areas of focal infiltrates. **d**, Intrathyroidal immune cell frequency among groups [isotype, *n*=11, except *n*=16 for $CD3^+$), Dual ICI (*n*=17, except *n*=23 for $CD3^+$), Dual ICI + αIL-17A (*n*=8)]. Data are mean ±SEM shown. *p<0.05, **p<0.01, ***p<0.001, ****p<0.0001. Brown-Forsythe ANOVA, assuming unequal s.d., followed by Dunnett's multiple comparisons test (**b, d**).

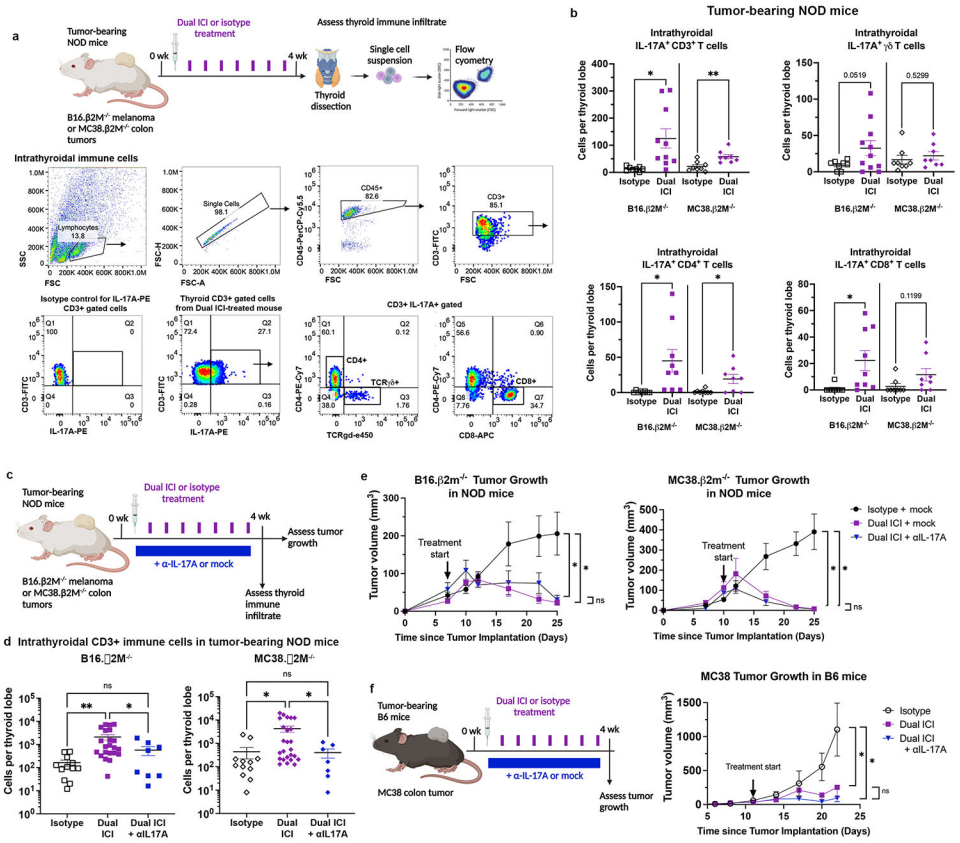

Figure 5. Contribution of IL-17A$^+$ T cells in ICI-associated thyroid autoimmune infiltrates in tumor-bearing NOD mice.

a, Schematic of ICI treatment and thyroid immune infiltrate assessment in tumor-bearing NOD mice (*top*). Representative dot plots and gating strategy for thyroid infiltrating immune cells (*bottom*). **b**, Quantification of intrathyroidal IL-17A$^+$ CD3$^+$ T cells and IL-17A$^+$ T cell subsets in tumor-bearing NOD mice by flow cytometry. Data shown as absolute cells per thyroid lobe; each dot represents one animal; stratified by tumor type. **c,** Schematic of ICI treatment with or without a neutralizing IL-17A (αIL-17A) antibody in tumor-bearing NOD mice for concurrent assessment on thyroid autoimmune infiltrate (IrAE) and tumor growth (ICI efficacy). **d**, Comparison of accumulation of intrathyroidal CD3$^+$ T cells in isotype, Dual ICI, or Dual ICI + αIL-17A by flow cytometry. Data shown as absolute cells per thyroid lobe; each dot represents one animal; stratified by tumor type. **e,** Growth of B16 β2M$^{-/-}$ and MC38. β2M$^{-/-}$ tumors in NOD mice treated with isotype for ICI (isotype) and isotype for αIL-17A (mock) (n=11-13), Dual ICI with mock (n=7), or Dual ICI with αIL-17A (n=8). **f,** Growth of syngeneic MC38 colon tumors in C57/B6 (B6) mice treated with isotype, Dual ICI, or Dual ICI and αIL17A, n=6-8 each group. Data are mean ±SEM shown. *p<0.05, **p<0.01, ***p<0.001, ****p<0.0001. Two-tailed, unpaired t test with Welch correction, assuming unequal s.d. and Holm-Sidak method correction for multiple comparisons (**b**); Brown-Forsythe ANOVA, assuming unequal s.d., followed by Dunnett's multiple comparisons test (**d**; comparison of day 25 tumor volume in **e;** comparison of day 22 tumor volume in **f**).